JACS
JOURNAL OF THE AMERICAN CHEMICAL SOCIETY
pubs.acs.org/JACS
Article

Element-Specific Donor Numbers for Anions

Lewis G. Parker, Frances K. Towers Tompkins, Jake M. Seymour, Ekaterina Gousseva, Christopher D. Smith, Roger A. Bennett, Pilar Ferrer, David C. Grinter, Claudia Kolbeck, Dennis Hein, Garlef Wartner, Robert Seidel, Denis Céolin, Robert Temperton, Robert G. Palgrave, Richard P. Matthews, and Kevin R. J. Lovelock*

Cite This: J. Am. Chem. Soc. 2026, 148, 35498−35514

Read Online

ACCESS | Metrics & More | Article Recommendations | Supporting Information

ABSTRACT: Anion interactions with cations/molecules are crucial across chemistry and biology: in battery electrolytes, synthesis, atmospheric processes, and protein denaturation. Selecting the optimum anion represents an immense challenge, as anion interactions are diverse and complex. Descriptors are needed that quantitatively capture the ability of anions to interact with cations and molecules. However, only a small number of experimental anion interaction descriptors exist, all with similar limitations. Here we show that core-level anion electron binding energies, E_B(core,anion), can be used to produce a new atomic-level descriptor for each of the key donor elements for anion interactions (O, N, F, Cl, Br, I, S), the element-specific donor number ($DN_{E\text{-}XPS}$). $DN_{E\text{-}XPS}$ descriptors are intrinsic, capturing the anion interaction abilities independent of any probe, countercation, or solvent. $DN_{E\text{-}XPS}$ descriptors are also interpretable, as E_B(core,anion) and therefore $DN_{E\text{-}XPS}$ are proportional to the electrostatic potential at the specific donor atom nucleus. Experimental core-level X-ray photoelectron spectroscopy (XPS) is used to measure E_B(core,anion) and therefore $DN_{E\text{-}XPS}$. Furthermore, $DN_{E\text{-}XPS}$ descriptors are produced easily and at low cost using lone-anion-SMD (solvation model density) calculations, a significant advance on the current anion descriptors, greatly reducing and potentially removing the need for experimental anion characterization. This work will greatly facilitate anion selection, especially for complex anions capable of forming interactions through multiple different atoms. We envisage our calculation method enabling the production of a very large database of $DN_{E\text{-}XPS}$ for each key element, ideal for use as machine learning training data sets.

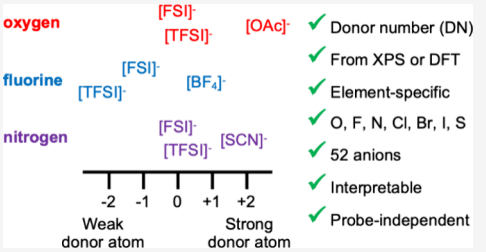

1. INTRODUCTION

Interactions of anions with cations/molecules/solids play a key role in a vast number of chemical, biological, and industrial processes. For energy storage devices,[1,2] anion−metal cation interactions in battery electrolytes can both ease metal cation desolvation before deposition/intercalation[3−5] and facilitate superior solid-electrolyte interphase (SEI) formation.[1,6−9] Furthermore, strong anion−solvent interactions in the battery electrolyte can enhance solvent reductive stability, reducing unwanted electrochemical decomposition.[10−12] In the realm of chemical synthesis,[13−20] the strength of anion−hydroxyl group interactions is an important factor for deconstruction of lignocellulosic biomass into biofuels.[13] Moreover, weakly coordinating anions are important for both (stereoselective) cationic catalysts[17,18] and stabilization of highly electrophilic/oxidizing cations.[16] Lastly, in the electrochemical synthesis of CO_2 for fuel production, anion−metal surface interactions significantly impact both kinetics and selectivity.[19,20] For biological processes,[21,22] protein denaturation can be directed by the strength of anion−protein interactions.[21]

Selecting the optimum anion for an application represents an immense challenge. The number of anions to choose from is large and growing.[23−29] Anion structures are diverse: from monatomic to large polyatomic; from highly symmetric to relatively asymmetric (examples in Figure 1). Anion interaction/binding modes to cations/molecules are complex. Most anions have multiple potential donor atoms and so can bind mono-/bi-/tridentate, depending on the solution composition, e.g., $[PF_6]^-$ with Li^+ can be mono-/bi-/tridentate.[30−34] A further complication can be anions that contain more than one type of donor atom (Figure 1 and Supporting Information Table S2); the primary (1°) donor atom will dominate anion interactions (e.g., O donor atoms for $[(CF_3SO_2)_2N]^-$), but strong interactions of secondary/tertiary (2°/3°) donor atoms are also influential, e.g., F donor atoms of $[(CF_3SO_2)_2N]^-$ for LiF formation in SEIs.[35,36]

Descriptors that quantify anion interactions are needed to rationalize and optimize anion selection. Historically, trial-and-error has been used to some extent to select good candidate

Received: March 30, 2026
Revised: June 30, 2026
Accepted: July 1, 2026
Published: August 13, 2026

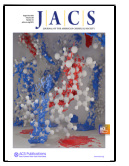

https://doi.org/10.1021/jacs.6c06567
J. Am. Chem. Soc. 2026, 148, 35498−35514

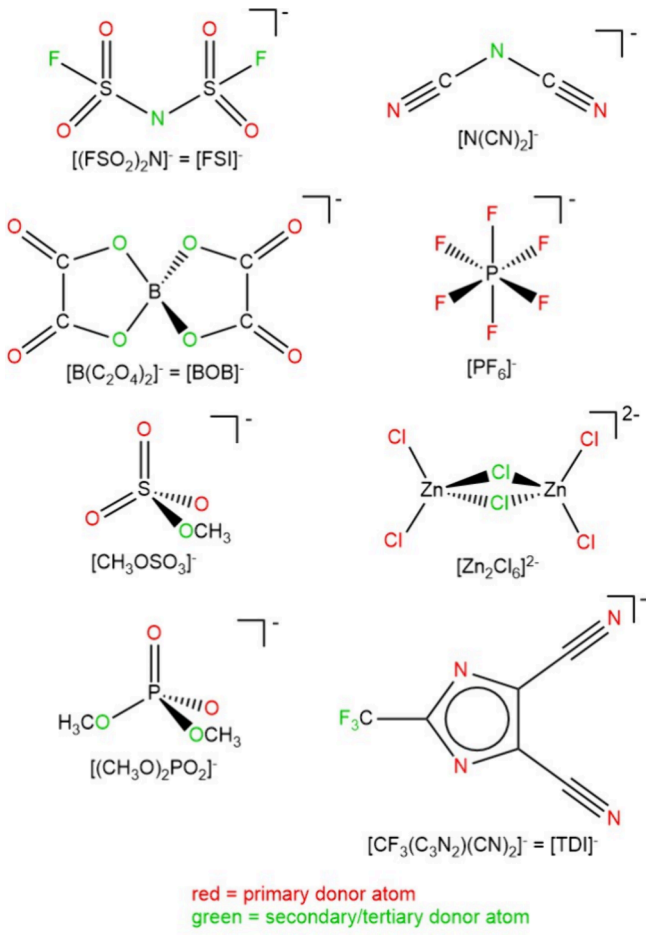

Figure 1. Selected anions with primary/secondary/tertiary (1°/2°/3°) donor atoms labeled.

anions.[37−41] More recently, data-driven methods have come to the fore.[37,42,43] Experimental anion descriptors based on the spectroscopy of anion-probe interactions, summarized in Table 1,[37,43−53] are now routinely used to aid anion selection, especially in the ionic liquid[13] and battery communities.[54−59] Probes used are either a cation (Na^+,[44] Li^+,[45] dialkylimidazolium cation,[46−49] Cu^+ complex[46]) to produce donor number (DN) descriptors or heterocyclic dye molecules to produce hydrogen bond acceptor (β) descriptors.[50−53] The most prominent of these anion descriptors were originally developed as solvent descriptors in the 1970s (Kamlet−Taft β_{KT}, and DN from ^{23}Na NMR, $DN_{Na\text{-}NMR}$),[60−62] highlighting that new interaction strength descriptors are rarely discovered. Furthermore, the current experimental anion descriptors have several critical limitations, as discussed in the next four paragraphs.

Anion descriptors are needed that provide atomic-level insights into interactions. For solvents, there has been a recent realization that single-value interaction strength descriptors do not provide atomic-level insight and are insufficient to capture interaction complexity.[63−68] For example, calculated electrostatic potential (ESP) descriptors are a recent and growing area in the battery community to identify which part of the solvent/additive molecule has good electron donor ability,[63,64] including the oxygen atom coordinated to Li^+.[68] Given that anion interactions are more complex than solvent interactions, the single value to describe the whole anion provided by the existing anion descriptors leaves significant room for improvement.

There is strong uncertainty over the general applicability of the current probe-dependent experimental anion descriptors. The anion-substrate interaction relevant to an application will often be very different to the anion-probe interaction captured by the anion descriptor.[66] Moreover, anion descriptors are probe-dependent (Table 1); probe-cation/probe-solvent interactions contribute (see Supporting Information section 1 for more details).[44,50−52] Thus, the current anion descriptors are not intrinsic measures of anion properties.[37,43−53] Intrinsic anion descriptors do not exist due to the limitations of the current spectroscopic toolbox; NMR, IR and Raman spectroscopies are all limited to certain elements/functional groups in anions, and the 1° donor atom for anions varies greatly, e.g., O in $[(CF_3\mathbf{S}O_2)_2N]^-$, F in $[\mathbf{P}F_6]^-$, N in $[B(\mathbf{C}N)_4]^-$, Cl in $[Zn\mathbf{Cl}_4]^{2-}$ (examples in Figure 1).

Expensive anion synthesis combined with descriptor measurement is currently essential to understand and predict anion interaction strengths. The existing experimental anion descriptors have not been calculated using high accuracy and low-cost methods. One attempt for anion β_{KT} concluded that their method, calculation of the spectroscopic signature of relatively large anion-probe structures, was not suitable for routine screening.[69] Furthermore, the accuracy of anion descriptors from low-cost calculations, e.g., Fukui functions,[70−72] is under question as they have not been validated against experimental anion descriptors; gas-phase lone-anion calculations generally do not capture liquid-phase anion properties.[73] Machine learning (ML) has been used to predict

Table 1. Strengths and Weaknesses of Experimental Anion Descriptors That Capture Intermolecular Anion−Cation/Anion−Molecule Interaction Strengths

descriptor	ref	spectroscopic method	probe	atomic-level?	probe-independent?	readily calculated?	interpretability
β_{KT}	50, 51	UV−vis	heterocyclic dye molecules	X	X	X	Reasonable
β_{NMR}	52	^{19}F NMR	fluorinated heterocyclic dye molecules	X	X	X	Reasonable
β_{titr}	53	UV−vis	heterocyclic dye molecules	X	X	X	Reasonable
$DN_{Na\text{-}NMR}$	44	^{23}Na NMR	Na^+	X	X	X	Challenging
$DN_{Li\text{-}NMR}$	45	^{7}Li NMR	Li^+	X	X	X	Very challenging
$DN_{Im\text{-}NMR}$	46, 47	^{1}H NMR	$[C_4C_1Im]^+$	X	X	X	Challenging
$DN_{Im\text{-}XPS}$	48, 49	XPS	$[C_8C_1Im]^+$	X	X	X	Excellent
$DN_{Cu\text{-}UV}$	46	UV−vis	cationic Cu complex	X	X	X	Reasonable
$DN_{E\text{-}XPS}$	here	XPS	no probe	√	√	√	Excellent

https://doi.org/10.1021/jacs.6c06567
J. Am. Chem. Soc. 2026, 148, 35498−35514

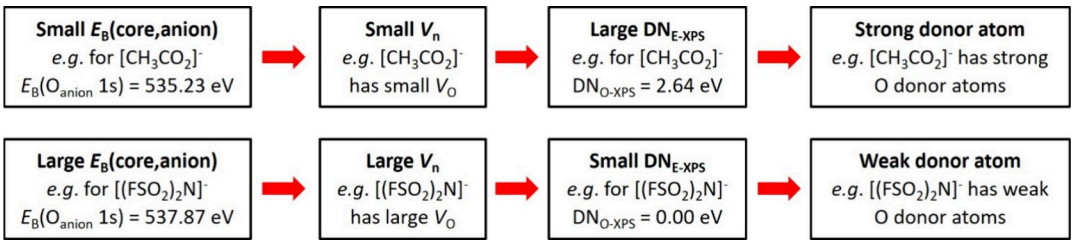

Figure 2. Relationship between XPS electron binding energies, E_B(core,anion), e.g., $E_B(O_{anion}\ 1s)$, electrostatic potential at the nucleus (as defined in ref 101), V_n, e.g., V_O, element-specific donor number, $DN_{E\text{-}XPS}$, e.g., $DN_{O\text{-}XPS}$, and donor atom strength/ability.

interaction strength descriptors for solvents/molecules[74−77] but not for anions to date.

For existing experimental anion descriptors, interpretability remains an issue; correlations between common/easily understood anion physicochemical properties and the experimental anion descriptors are sorely lacking (Table 1). This is caused by the same problems that limit calculations: lack of understanding of both the specific anion-probe interactions and the spectroscopies (especially NMR[78−80]). Interpretable experimental anion descriptors can provide a route to design rules for anion selection.

Here we use the element specificity of core-level X-ray photoelectron spectroscopy (XPS),[81] along with easy and low-cost DFT calculations, to obtain core-level anion electron binding energies, E_B(core,anion), for key elements for anion electron donation (O, N, F, Cl, Br, I, S). Both liquid-jet XPS apparatus (for anions in molecular solvents) and liquid drop apparatus (for anions in ionic liquids) are used to experimentally measure E_B(core,anion). Lone-anion SMD (solvation model density) calculations are used to calculate E_B(core,anion). We then convert these E_B(core,anion) into new element-specific donor number ($DN_{E\text{-}XPS}$) descriptors for 52 anions in total across the seven elements (Supporting Information Table S2). For E_B(core,anion) in ionic liquids, we use a combination of data measured here and literature data;[48,73,82−95] the focus of literature studies involving E_B(core,anion) has previously been anion speciation[86,92] and not anion descriptor generation. Here we provide the first XPS measurements for the same anions in different molecular solvents and make crucial comparisons to XPS for anions in ionic liquids for the first time. There is little E_B(core,anion) data for anions solvated in molecular solvents;[96,97] the focus has been on E_B(valence,anion) for anions in water.[98−100] E_B(core,anion) and therefore $DN_{E\text{-}XPS}$ have the potential to capture anion interaction strength.[101] The 52 anions (Supporting Information Table S2) are chosen based on a combination of relevance to specific applications (batteries, synthesis and catalysis, atmospheric chemistry, gas capture, and protein denaturation) and covering the range of possible donor atom types. The solvents studied here cover an excellent range of solvation environments; water is a good electron acceptor solvent, whereas triethyl phosphate (TEP), propylene carbonate (PC), and dialkylimidazolium (the countercation used here for ionic liquids) are relatively poor electron acceptors.[102,103]

2. RESULTS AND DISCUSSION

2.1. Element-Specific Anion Donor Number Values: Atomic-Level Descriptors

We have measured XPS-derived element-specific donor numbers, $DN_{E\text{-}XPS}$, for the first time. $DN_{E\text{-}XPS}$ provide experimental atomic-level descriptors for primary/secondary/tertiary (1°/2°/3°) donor atoms for anions. Small E_B(core,anion) → small V_n (V_n is the electrostatic potential at the nucleus, where n is the nucleus of a specific atom) → large $DN_{E\text{-}XPS}$ → strong donor atom (Figure 2, top). In contrast, large E_B(core,anion) → large V_n → small $DN_{E\text{-}XPS}$ → weak donor atom (Figure 2, bottom).

As this publication represents the first time that XPS has been used to obtain $DN_{E\text{-}XPS}$, here we show exemplar O_{anion} 1s XP spectra used to obtain $DN_{O\text{-}XPS}$ for seven anions in ionic liquids (Figure 3, Supporting Information Figure S56 for O_{anion} 1s XP spectra of all 15 anions studied here). In core-level XPS, different covalent bonding environments can be distinguished for the same element in a single anion given sufficiently different E_B(core,anion); peak area ratios for the same element match the stoichiometry of the anion, which allows the contributions from anion structural moieties to be identified in the experimental XP spectra. The two different O atom bonding environments in $[ROSO_3]^-$ (R = H, CH_3, C_8H_{17}), 1° donor SO_3 and 2° donor RO (structure for R = CH_3 in Figure 1), are well-separated in $E_B(O_{anion}\ 1s)$ and in a 3:1 area ratio (Figure 3 and Supporting Information Figure S56); $E_B(O_{anion}$ 1s) and therefore $DN_{O\text{-}XPS}$ can be measured for both SO_3 and RO. Different covalent bonding environments can be distinguished for other anions: O_{PO} and O_{OC} in $[(CH_3O)_2PO_2]^-$ (structure in Supporting Information Table S2, XP spectrum in Supporting Information Figure S56), $N_{terminal}$ and $N_{bridging}$ in $[N(CN)_2]^-$ (structure in Figure 1, XP spectrum in Supporting Information Figure S57), F_{PF} and F_{CF} in $[(C_2F_5)_3PF_3]^-$ (structure in Supporting Information Table S2, XP spectrum in Supporting Information Figure S58), terminal and bridge halides in halozincates (example structure in Figure 1, XP spectra in Supporting Information Figures S59 and S60). Furthermore, anions that are too challenging to measure for other experimental descriptors (e.g., I^- or open-shell metal complexes for β based on UV−vis spectroscopy) can be measured using core-level XPS. Calculations can facilitate identification of atoms of the same element with different covalent bonding with similar donor strength in the same anion, which is very challenging for experimental XPS, e.g., for oxygen in $[B(C_2O_4)_2]^-$ (structure in Figure 1), O_{BO} and O_{CO} bonding environments can be readily distinguished in the calculated O 1s XP spectrum (Figure 3, structure in Figure 1).

For four of the 52 anions studied here ($[(CF_3SO_2)_2N]^-$ (also known as $[NTf_2]^-$ or $[TFSI]^-$), $[(C_2F_5SO_2)_2N]^-$ (also known as $[NPf_2]^-$ or $[BETI]^-$), $[(FSO_2)_2N]^-$ (also known as $[FSI]^-$), and $[SCN]^-$), the identity of the primary donor atom depends on the cation/molecule the anion is interacting with, e.g., O or N for $[(CF_3SO_2)_2N]^-$. We have identified the primary donor atom for these four anions as the atom type that

https://doi.org/10.1021/jacs.6c06567
J. Am. Chem. Soc. 2026, 148, 35498−35514

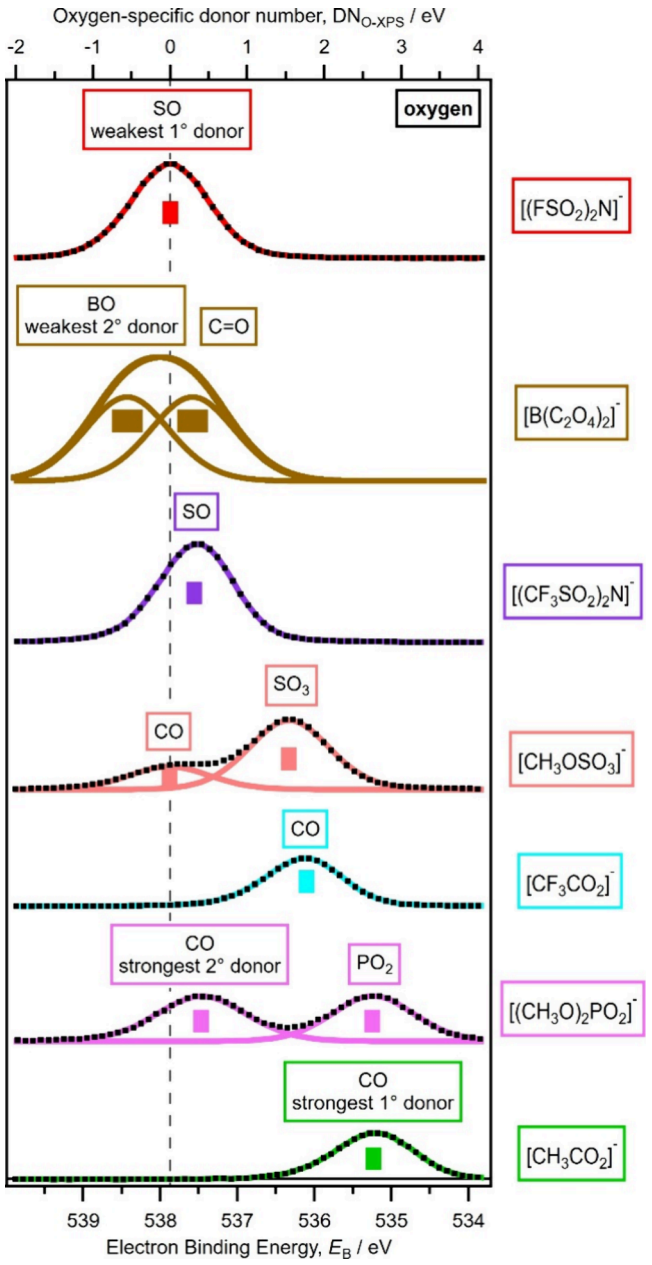

Figure 3. O 1s XP spectra (dots are XP spectra, colored traces are fits) and values of $E_B(O_{anion}\ 1s)$ and DN_{O-XPS} (bottom and top axes, respectively) of oxygen-containing anions in ionic liquid: $[C_8C_1Im][(FSO_2)_2N]$; $[B(C_2O_4)_2]^-$ (total and also calculated C═O and BO contributions); $[C_8C_1Im][(CF_3SO_2)_2N]$; $[C_4C_1Im][CH_3OSO_3]$ (total and also fitted CO and SO_3 components); $[C_8C_1Im][CF_3CO_2]$; $[C_4C_1Im][(CH_3O)_2PO_2]$ (total and also fitted CO and PO_2 components); $[C_4C_1Im][CH_3CO_2]$. Traces are vertically offset for clarity. Area normalization is to the number of atoms in each anion and explained further in Supporting Information section 8.3. Charge referencing is given in Supporting Information section 8.2. For $E_B(O_{anion}\ 1s)$ (and therefore DN_{O-XPS}), the experimental uncertainty is ±0.10 eV (Supporting Information section 14.2) and the calculated uncertainty is ±0.20 eV (Supporting Information section 14.4); these uncertainty values are represented by the width of each block.

most commonly interacts with cations/molecules using a combination of experiments[104−106] and calculations:[35] O for $[(CF_3SO_2)_2N]^-$, $[(C_2F_5SO_2)_2N]^-$, and $[(FSO_2)_2N]^-$; N for $[SCN]^-$.

DN_{E-XPS} values for seven elements are each produced using the same method (see Figure S9 and Figure S10 for two flowcharts explaining the method in detail). Values of DN_{E-XPS} for each element are obtained using a combination of E_B(core,anion) (Supporting Information Figures S56−S62) and the appropriate equation (Table 2, column 2); DN_{E-XPS} values are given in Table 3 to Table 6, Supporting Information Tables S52−S54). The equations for DN_{E-XPS} (Table 2, column 2) are produced using E_B(core,anion) for the weakest 1° donor atom for each element (anion identified in Table 2, column 3, E_B(core,anion) value given in Table 2, column 4). For example, $[(FSO_2)_2N]^-$ is the weakest 1° oxygen donor atom presented here, giving the largest $E_B(O_{anion}\ 1s)$ for a 1° oxygen donor atom, $E_B(O_{anion}\ 1s)$ = 537.87 eV. Therefore, $[(FSO_2)_2N]^-$ is set to DN_{O-XPS} = 0 eV to produce the equation for oxygen in Table 2, row 2 (see top axis on Figure 3, dashed vertical line represents DN_{O-XPS} = 0 eV and Figure 2), We chose not to scale DN_{E-XPS} between 0 (weakest donor) and 1 (strongest donor), e.g., as is done for β_{KT}, because ΔDN_{E-XPS} are directly related to ΔV_n (see section 2.4).

The strongest donor atoms have the largest positive DN_{E-XPS} value for that element (Figure 2, Tables 3−6, Supporting Information Tables S52−S54). For example, the strongest O_{anion} donor atoms are in $[(CH_3O)_2PO_2]^-$ and $[CH_3CO_2]^-$, with DN_{O-XPS} of 2.63 and 2.64 eV respectively (Figure 2, Figure 3 top axis, Table 3 and Supporting Information Figure S56). Given our choice here of setting DN_{E-XPS} = 0 eV for the weakest 1° donor atom, negative values of DN_{E-XPS} only occur for 2°/3° donor atoms; the weakest donor atoms have the largest negative DN_{E-XPS} value for that element. In the future, negative values of DN_{E-XPS} are likely to be found for very weakly interacting 1° donor atoms once more anions are studied using this method. For example, DN_{O-XPS} = −0.56 eV is the smallest value for oxygen, for the BO oxygen 2° donor atoms in $[B(C_2O_4)_2]^-$ (structure in Figure 1, DN_{O-XPS} in Table 3, top axis on Figure 3 and Supporting Information Figure S56).

We chose to use ionic liquids here as the principal solvent environment for producing DN_{E-XPS} (rather than molecular solvents, e.g., see section 2.2) for three major reasons. First, $E_B(O_{anion}\ 1s)$ can be measured for all O-containing anions in ionic liquids. For many molecular solvents (e.g., water, PC, TEP), the $O_{solvent}$ 1s contribution obscures the O_{anion} 1s contribution (e.g., O 1s graphs for 18 samples in Supporting Information sections 11−13), meaning measurement of $E_B(O_{anion}\ 1s)$ in most molecular solvents is very challenging and potentially impossible, certainly at low anion concentration. Second, the existing E_B(core,anion) literature data sets for ionic liquids can be combined with new data measured here;[48,73,82−95] ionic liquids can be readily studied using standard XPS apparatus due to their very low vapor pressures.[107−109] Third, the anion makes up half the solution (or one-third for 2− anions), so solubility/contaminant issues that occur for the current probe-dependent anion descriptors (e.g., any colored contaminant for UV−vis spectroscopy) are far less of a problem for DN_{E-XPS} from ionic liquids.

2.2. Anion Element-Specific Donor Numbers: Intrinsic Measures of Anion Donor Abilities

Intrinsic anion donor abilities are captured by E_B(core,anion) and therefore DN_{E-XPS}, with excellent independence from the solvation environment and spectroscopic contributions. Intra-anion covalent bonding contributions dominate over non-

https://doi.org/10.1021/jacs.6c06567
J. Am. Chem. Soc. 2026, 148, 35498−35514

Table 2. Summary of Equations and Data for Element-Specific Donor Numbers from XPS, $DN_{E\text{-}XPS}$

element	equation for $DN_{E\text{-}XPS}$	anion with largest E_B(core,anion) for 1° donor atoms	largest E_B(core,anion) for 1° donor atoms/eV
O	$DN_{O\text{-}XPS} = 537.87 - E_B(O_{anion}\ 1s)$	$[(FSO_2)_2N]^-$	537.87
N	$DN_{N\text{-}XPS} = 404.60 - E_B(N_{anion}\ 1s)$	$[B(CN)_4]^-$	404.60
F	$DN_{F\text{-}XPS} = 691.59 - E_B(F_{anion}\ 1s)$	$[PF_6]^-$	691.59
Cl	$DN_{Cl\text{-}XPS} = 204.39 - E_B(Cl_{anion}\ 2p_{3/2})$	$[GaCl_4]^-$	204.39
Br	$DN_{Br\text{-}XPS} = 74.42 - E_B(Br_{anion}\ 3d_{5/2})$	$[InBr_4]^-$	74.42
I	$DN_{I\text{-}XPS} = 624.15 - E_B(I_{anion}\ 3d_{5/2})$	$[I_3]^-$	624.15
S	$DN_{S\text{-}XPS} = 167.93 - E_B(S_{anion}\ 2p_{3/2})$	$[Co(NCS)_4]^{2-}$	167.93

Table 3. Experimental (Nonitalicized entries) And Calculated (Italicized Entries, Taken from Table S35) $E_B(O_{anion}\ 1s)$ and Oxygen-Specific Donor Numbers ($DN_{O\text{-}XPS}$) for Ionic Liquid Samples[a]

anion	moiety	1°/2°/3°	$E_B(O_{anion}\ 1s)$/eV	$DN_{O\text{-}XPS}$/eV
$[CH_3CO_2]^-$	O	Strongest 1°	535.23 ± 0.10	2.64 ± 0.10
$[(CH_3O)_2PO_2]^-$	O_{PO}	1°	535.25 ± 0.10	2.62 ± 0.10
$[CH_3SO_3]^-$	O	1°	536.05 ± 0.10	1.82 ± 0.10
$[CH_3C_6H_4SO_3]^-$	*O*	*1°*	*536.06 ± 0.20*	*1.81 ± 0.20*
$[CF_3CO_2]^-$	O	1°	536.10 ± 0.10	1.77 ± 0.10
$[C_8H_{17}OSO_3]^-$	O_{SO}	1°	536.28 ± 0.10	1.59 ± 0.10
$[CH_3OSO_3]^-$	O_{SO}	1°	536.33 ± 0.10	1.54 ± 0.10
$[HOSO_3]^-$	O_{SO}	1°	536.48 ± 0.10	1.39 ± 0.10
$[CF_3SO_3]^-$	O	1°	536.74 ± 0.10	1.13 ± 0.10
$[NO_3]^-$	O	1°	536.95 ± 0.10	0.92 ± 0.10
$[(CF_3SO_2)_2N]^-$	O	1°	537.56 ± 0.10	0.31 ± 0.10
$[(C_2F_5SO_2)_2N]^-$	O	1°	537.56 ± 0.10	0.31 ± 0.10
$[ClO_4]^-$	*O*	*1°*	*537.57 ± 0.20*	*0.30 ± 0.20*
$[B(C_2O_4)_2]^-$	*O_{CO}*	*1°*	*537.58 ± 0.20*	*0.29 ± 0.20*
$[(FSO_2)_2N]^-$	O	Weakest 1°	537.87 ± 0.10	0.00 ± 0.10
$[(CH_3O)_2PO_2]^-$	O_{OC}	Strongest 2°	537.47 ± 0.10	0.40 ± 0.10
$[C_8H_{17}OSO_3]^-$	O_{OC}	2°	537.71 ± 0.10	0.16 ± 0.10
$[HOSO_3]^-$	O_{OH}	2°	537.88 ± 0.10	−0.01 ± 0.10
$[CH_3OSO_3]^-$	O_{OC}	2°	537.88 ± 0.10	−0.01 ± 0.10
$[B(C_2O_4)_2]^-$	*O_{BO}*	*Weakest 2°*	*538.43 ± 0.20*	*−0.56 ± 0.20*

[a]Experimental uncertainties are ±0.10 eV (Supporting Information section 14.2), and calculated uncertainties are ±0.20 eV (Supporting Information section 14.4).

Table 4. Experimental (Nonitalicized Entries) And Calculated (Italicized Entries, Taken from Table S36) $E_B(N_{anion}\ 1s)$ and Nitrogen-Specific Donor Numbers ($DN_{N\text{-}XPS}$) for Ionic Liquid Samples[a]

anion	moiety	1°/2°/3°	$E_B(N_{anion}\ 1s)$/eV	$DN_{N\text{-}XPS}$/eV
$[(CH)_2N_2CH]^-$	*N*	*Strongest 1°*	*402.49 ± 0.20*	*2.11 ± 0.20*
$[C_6H_4N_2CH]^-$	*N*	*1°*	*402.64 ± 0.20*	*1.96 ± 0.20*
$[SCN]^-$	N	1°	402.66 ± 0.10	1.94 ± 0.10
$[N(CN)_2]^-$	$N_{terminal}$	1°	403.21 ± 0.10	1.39 ± 0.10
$[C(CN)_3]^-$	N	1°	403.69 ± 0.10	0.91 ± 0.10
$[CF_3(C_3N_2)(CN)_2]^-$	*N_{ring}*	*1°*	*404.18 ± 0.20*	*0.42 ± 0.20*
$[CF_3(C_3N_2)(CN)_2]^-$	*N_{CN}*	*1°*	*404.24 ± 0.20*	*0.36 ± 0.20*
$[B(CN)_4]^-$	N	Weakest 1°	404.60 ± 0.10	0.00 ± 0.10
$[(CF_3SO_2)_2N]^-$	N	Strongest 2°	404.32 ± 0.10	0.28 ± 0.10
$[(C_2F_5SO_2)_2N]^-$	N	2°	404.32 ± 0.10	0.28 ± 0.10
$[N(CN)_2]^-$	N_{bridge}	2°	404.50 ± 0.10	0.10 ± 0.10
$[(FSO_2)_2N]^-$	N	Weakest 2°	404.64 ± 0.10	−0.04 ± 0.10

[a]Experimental uncertainties are ±0.10 eV (Supporting Information section 14.2), and calculated uncertainties are ±0.20 eV (Supporting Information section 14.4).

covalent solvation effects (anion-molecule or anion-counter-cation) and different anion solvation at the liquid−gas surface (see Supporting Information section 32). The intrinsic nature of $DN_{E\text{-}XPS}$ is reinforced by the calculation results presented in section 2.3. In the field of Lewis acids and Lewis bases, it has been assumed that intrinsic Lewis acidity or intrinsic Lewis basicity can only be captured using calculations;[110,111] we show that intrinsic anion donor ability (very closely related to intrinsic anion Lewis basicity) can be measured using experiments.

There are excellent visual matches of both the E_B(core,anion) order and ΔE_B(core,anion) for anions in water, ionic liquid, PC and TEP (Figure 4 for F_{anion} 1s and Figure 5 for N_{anion} 1s). For example, the $E_B(N_{anion}\ 1s)$ order in

https://doi.org/10.1021/jacs.6c06567
J. Am. Chem. Soc. 2026, 148, 35498−35514

Table 5. Experimental (Nonitalicized Entries) and Calculated (Italicized Entries, Taken from Table S37) $E_B(F_{anion}\ 1s)$ and Fluorine-Specific Donor Numbers ($DN_{F\text{-}XPS}$) for Ionic Liquid Samples[a]

anion	moiety	1°/2°/3°	$E_B(F_{anion}\ 1s)$/eV	$DN_{F\text{-}XPS}$/eV
$[BF_4]^-$	F	Strongest 1°	690.76 ± 0.10	0.83 ± 0.10
$[SbF_6]^-$	F	1°	691.05 ± 0.15	0.54 ± 0.15
$[(C_2F_5)_3PF_3]^-$	F_{PF}	1°	691.58 ± 0.10	0.01 ± 0.10
$[PF_6]^-$	F	Weakest 1°	691.59 ± 0.10	0.00 ± 0.10
$[(FSO_2)_2N]^-$	F	Strongest 2°/3°	692.66 ± 0.10	−1.07 ± 0.10
$[CF_3CO_2]^-$	F	2°	693.03 ± 0.10	−1.44 ± 0.10
$[CF_3(C_3N_2)(CN)_2]^-$	*F*	*2°/3°*	*693.14 ± 0.20*	*−1.55 ± 0.20*
$[CF_3SO_3]^-$	F	2°	693.23 ± 0.10	−1.64 ± 0.10
$[(C_2F_5)_3PF_3]^-$	F_{CF}	2°	693.23 ± 0.10	−1.64 ± 0.10
$[(CF_3SO_2)_2N]^-$	F	2°/3°	693.77 ± 0.10	−2.18 ± 0.10
$[(C_2F_5SO_2)_2N]^-$	F	Weakest 2°/3°	693.86 ± 0.10	−2.27 ± 0.10

[a]Experimental uncertainties are ±0.10 eV (apart from the $[SbF_6]^-$ anion with ±0.15 eV, Supporting Information section 14.2), and calculated uncertainties are ±0.20 eV (Supporting Information section 14.4).

Table 6. Experimental (Nonitalicized Entries) And Calculated (Italicized Entries, Taken from Table S38) $E_B(Cl_{anion}\ 2p_{3/2})$ and Chlorine-Specific Donor Numbers ($DN_{Cl\text{-}XPS}$) for Ionic Liquid Samples[a]

anion	moiety	1°/2°/3°	$E_B(Cl_{anion}\ 2p_{3/2})$/eV	$DN_{Cl\text{-}XPS}$/eV
Cl^-	Cl	Strongest 1°	201.84 ± 0.10	2.55 ± 0.10
$[LiCl_3]^{2-}$	Cl	1°	202.42 ± 0.20	1.97 ± 0.20
$[ZnCl_4]^{2-}$	Cl	1°	203.01 ± 0.10	1.38 ± 0.10
$[NiCl_4]^{2-}$	Cl	1°	203.01 ± 0.10	1.38 ± 0.10
$[CoCl_4]^{2-}$	Cl	1°	203.03 ± 0.10	1.36 ± 0.10
$[FeCl_4]^{2-}$	Cl	1°	203.05 ± 0.10	1.34 ± 0.10
$[Bi_2Cl_8]^{2-}$	Cl	1°	203.32 ± 0.10	1.07 ± 0.10
$[SnCl_3]^-$	Cl	1°	203.43 ± 0.10	0.96 ± 0.10
$[Zn_2Cl_6]^{2-}$	$Cl_{terminal}$	1°	203.50 ± 0.15	0.89 ± 0.15
$[Zn_3Cl_8]^{2-}$	$Cl_{terminal}$	1°	203.65 ± 0.15	0.74 ± 0.15
$[Zn_4Cl_{10}]^{2-}$	$Cl_{terminal}$	1°	203.72 ± 0.15	0.67 ± 0.15
$[InCl_4]^-$	Cl	1°	204.23 ± 0.10	0.16 ± 0.10
$[FeCl_4]^-$	Cl	1°	204.25 ± 0.15	0.14 ± 0.15
$[AlCl_4]^-$	*Cl*	*1°*	*204.27 ± 0.20*	*0.12 ± 0.20*
$[GaCl_4]^-$	*Cl*	*Weakest 1°*	*204.39 ± 0.20*	*0.00 ± 0.20*
$[Zn_2Cl_6]^{2-}$	Cl_{bridge}	Strongest 2°	204.20 ± 0.15	0.19 ± 0.15
$[Zn_3Cl_8]^{2-}$	Cl_{bridge}	2°	204.51 ± 0.15	−0.12 ± 0.15
$[Zn_4Cl_{10}]^{2-}$	Cl_{bridge}	Weakest 2°	204.66 ± 0.15	−0.27 ± 0.15

[a]Experimental uncertainties are ±0.10 eV (apart from the oligomeric chlorozincate and $[FeCl_4]^-$ anions with ±0.15 eV, $[LiCl_3]^-$ anion with ±0.20 eV, Supporting Information section 14.2), and calculated uncertainties are ±0.20 eV (Supporting Information section 14.4).

all four solvents is $[(FSO_2)_2N]^-$ > $[(CF_3SO_2)_2N]^-$ > $[SCN]^-$ (Figure 5); $E_B(N_{anion}\ 1s)$ for both types of donor nitrogen atom in $[N(CN)_2]^-$ also appear in the same order for water and ionic liquid (Figure 5). Furthermore, there are excellent linear correlations (R^2 very near 1 and gradients close to 1) for $E_B(F_{anion}\ 1s)$ in different solvents, e.g., ionic liquid versus water (Figure 6a), and also $E_B(N_{anion}\ 1s)$ in different solvents, e.g., ionic liquid versus water (Figure 6c).

We have high confidence that any solvent, beyond those studied here, will not have a strong effect on ΔE_B(core,anion) and therefore $\Delta DN_{E\text{-}XPS}$. The four different solvents studied here give an excellent range of solvent acceptor numbers, i.e., the abilities of the solvents studied here to interact with the anion are not the same. Water is a strong electron acceptor; PC, TEP and most ionic liquids are midrange to weak electron acceptors.[102]

Countercation effects on E_B(core,anion) and therefore $DN_{E\text{-}XPS}$ in molecular solvents, i.e., changing the cation and keeping the anion $[A]^-$ the same, are within the experimental uncertainty at relatively low salt concentration (≤1 M). We have substantial data for same anion-different countercations samples for all three molecular solvents studied here (Supporting Information Figures S63−S67). The countercations studied have very different interaction properties/strengths: large, organic $[C_4C_1Im]^+$ versus small inorganic M^+ (Li^+, Na^+, K^+) versus small inorganic M^{2+} (Mg^{2+}, Ca^{2+}, Zn^{2+}). For example, [cation][CF_3SO_3] in water was studied with six different countercations (Na^+, K^+, Mg^{2+}, Ca^{2+}, Zn^{2+}, $[C_4C_1Im]^+$, Supporting Information Figure S64); [cation][SCN] in PC with two different countercations (K^+, $[C_4C_1Im]^+$, Supporting Information Figure S65); [cation][$(CF_3SO_2)_2N$] in TEP with two different countercations (Li^+, Na^+, Supporting Information Figure S67). At higher salt concentrations, e.g., 8 M, countercation effects are likely to become important.

For ionic liquids, the effect of the organic dialkylimidazolium countercation, $[C_nC_1Im]^+$, with different n values (i.e., different alkyl chain substituent lengths) on E_B(core,anion) and therefore $DN_{E\text{-}XPS}$ is within the experimental uncertainty.[73,84] In contrast, the alkyl chain substituent length n had

https://doi.org/10.1021/jacs.6c06567
J. Am. Chem. Soc. 2026, 148, 35498−35514

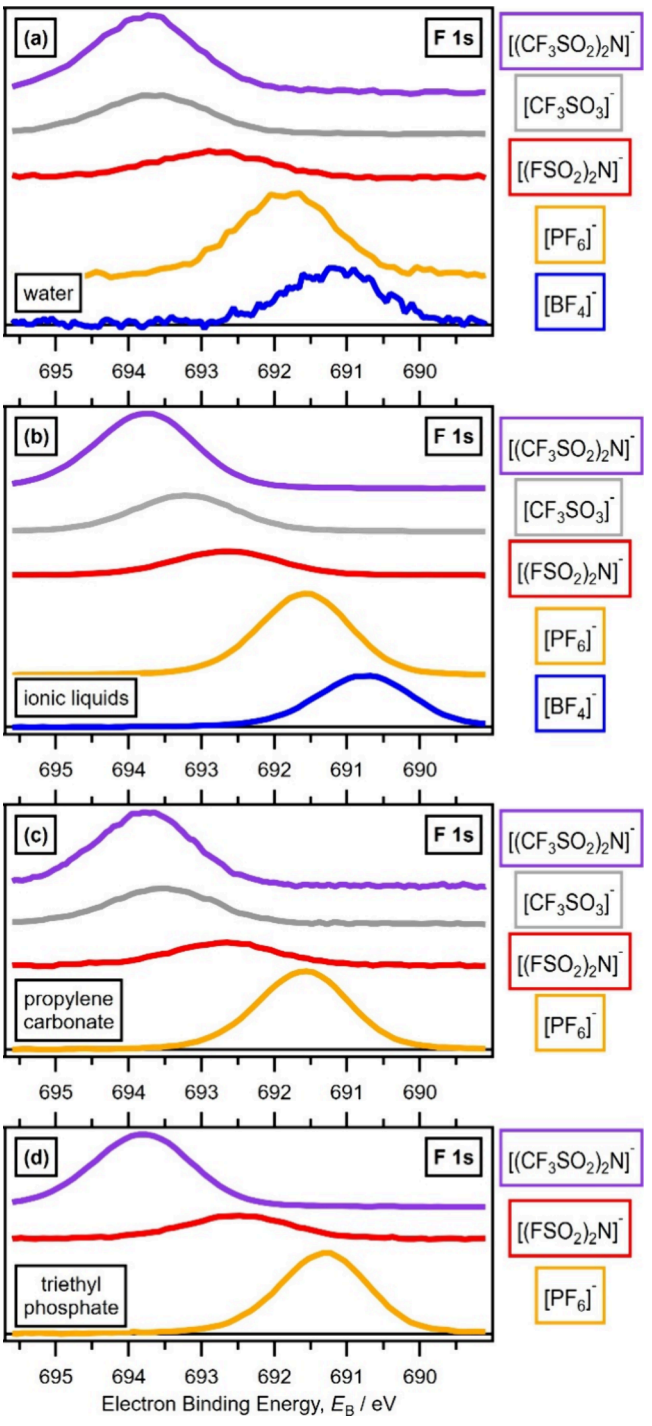

Figure 4. Comparison of fluorine-containing anions in different solvation environments. (a) F 1s XPS of fluorine-containing anions in water: 0.50 M $Li[(CF_3SO_2)_2N]$, 0.40 M $Na[CF_3SO_3]$, 0.40 M $Na[(FSO_2)_2N]$, 0.50 M $Li[PF_6]$, 0.50 M $[C_4C_1Im][BF_4]$. (b) F 1s XPS of fluorine-containing anions in ionic liquid: $[C_8C_1Im][(CF_3SO_2)_2N]$, $[C_8C_1Im][CF_3SO_3]$, $[C_8C_1Im][(FSO_2)_2N]$, $[C_8C_1Im][PF_6]$, $[C_8C_1Im][BF_4]$. (c) F 1s XPS of fluorine-containing anions in propylene carbonate: 0.14 M $Li[(CF_3SO_2)_2N]$, 0.15 M $Na[CF_3SO_3]$, 0.30 M $Na[(FSO_2)_2N]$, 0.50 M $Li[PF_6]$. (d) F 1s XPS of fluorine-containing anions in triethyl phosphate: 0.48 M $Li[(CF_3SO_2)_2N]$, 0.50 M $Na[(FSO_2)_2N]$, 0.50 M $Li[PF_6]$. Traces are vertically offset for clarity. Area normalization is to the number of atoms in each anion and explained further in Supporting Information section 8.3. Charge referencing: water $E_B(O_{liquid}\ 1s)$ = 538.13 eV; ionic liquid $E_B(C_{alkyl}\ 1s)$ = 289.85 eV; propylene carbonate $E_B(C_{carbonyl}\ 1s)$ = 295.80 eV; triethyl phosphate $E_B(C_{alkyl}\ 1s)$ = 290.32 eV (see Supporting Information section 8.1 for more details).

an impact on anion $DN_{Na\text{-}NMR}$ measured using ^{23}Na NMR spectroscopy in different $[C_nC_1Im][A]$ ionic liquids. This literature finding is perhaps surprising given that the $[C_nC_1Im]^+$ cations are not directly solvating the Na^+ cation, i.e., Na^+ will have anions in the first solvation shell and $[C_nC_1Im]^+$ cations in the second solvation shell. The differing countercation dependencies for $DN_{E\text{-}XPS}$ versus $DN_{Na\text{-}NMR}$ may be due to the spectroscopic time scales of core-level XPS and NMR spectroscopy; nuclear motion could be important for NMR spectroscopy, whereas photoemission in XPS is sufficiently fast ($\sim 10^{-15}$ s) that nuclear motion during the spectroscopic event will be negligible.

Our intrinsic $DN_{O\text{-}XPS}$ for 1° oxygen atoms show excellent matches to (single-value) literature anion-level descriptors, demonstrating that, despite being measured using probes, the anion-level descriptors do a good job of capturing intrinsic anion donor ability. $DN_{O\text{-}XPS}$ give excellent/good linear correlations with eight different anion-level DN/β descriptors (range of R^2 0.97 to 0.70, Figure 6e and Figure 6f for two comparisons, Supporting Information Figure S71 for all eight comparisons).[44,46−51,53,112] For example, excellent linear correlations are found between $DN_{O\text{-}XPS}$ and both anion DNs (e.g., $DN_{Na\text{-}NMR}$,[44] Figure 6e) and anion β (e.g., β_{KT},[51] Figure 6f). These eight anion-level descriptors include a range of probes (metal cations, organic cations and molecules), giving high confidence that our 1° $DN_{O\text{-}XPS}$ and anion-level descriptors both capture donor ability. There is clearly some influence of the countercation on probe-dependent, anion-level DNs and β (see section 2.2), but when the same cation is used anion-level probe-dependent descriptors are primarily driven by intrinsic anion donor properties. For both $E_B(N_{anion}\ 1s)$ and $E_B(F_{anion}\ 1s)$, there is insufficient data for meaningful linear correlations to be obtained (see Supporting Information section 33 for more comment on this area).

By comparing probe-independent $DN_{E\text{-}XPS}$ against probe-dependent descriptors, there is an opportunity to learn more about probe-specific interactions. Differences in experimental $DN_{E\text{-}XPS}$ are driven by anion electronic properties, with minimal contributions from specific anion-probe binding or steric hindrance. In contrast, for the eight different anion-level DN/β descriptors specific anion-probe binding interactions provide an unknown contribution that is potentially probe-dependent and therefore anion-dependent. For a linear correlation between our $DN_{E\text{-}XPS}$ and an anion-level descriptor, any anion data point outside the experimental uncertainty could indicate a different anion-probe binding mechanism for that anion compared to the other anions studied (e.g., nitrogen dominated binding for $[(CF_3SO_2)_2N]^-$) or highlight the importance of steric hindrance. However, the lack of experimental uncertainty provision for most existing anion descriptors makes this approach challenging, and we will not pursue any such analysis here.

2.3. Lone-Ion-SMD Calculations Can Accurately and Efficiently Predict Anion Element-Specific Donor Numbers

The goal of E_B(core,anion) and therefore $DN_{E\text{-}XPS}$ prediction with high accuracy and low computational cost is achieved. Calculated $DN_{E\text{-}XPS}$ can be used with high confidence in

https://doi.org/10.1021/jacs.6c06567
J. Am. Chem. Soc. 2026, 148, 35498−35514

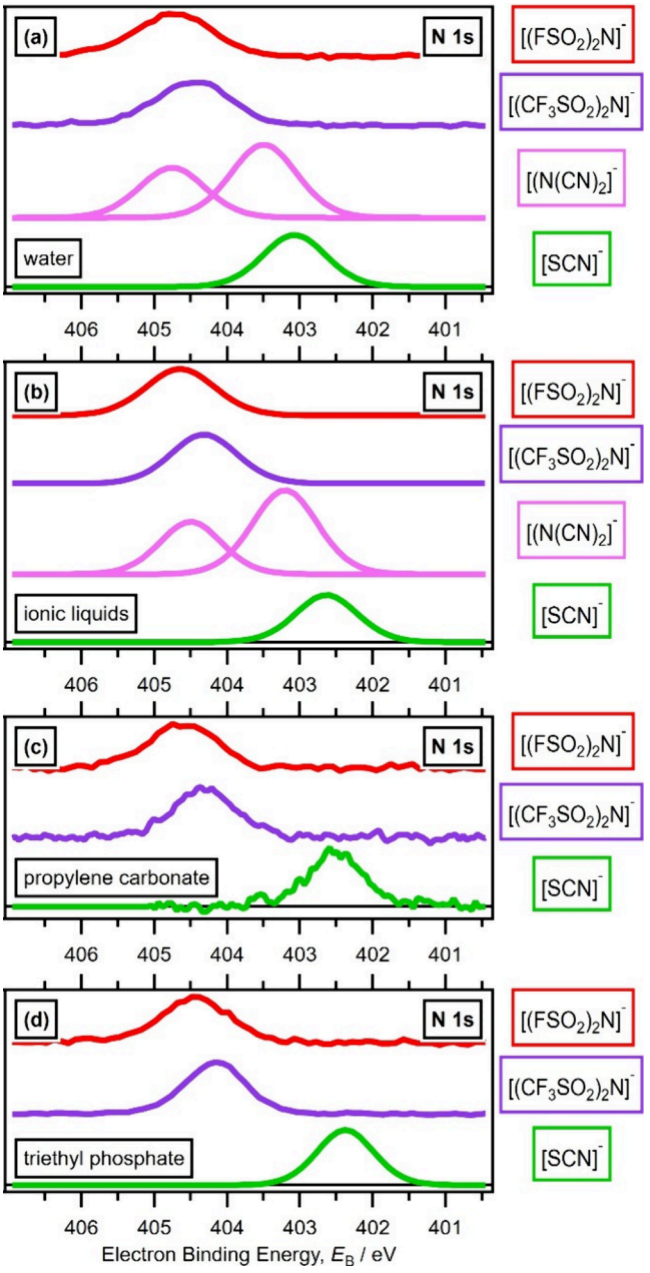

Figure 5. Comparison of nitrogen-containing anions in different solvation environments. (a) N 1s XPS of nitrogen-containing anions in water: 0.40 M Na[$(FSO_2)_2N$], 0.50 M Li[$(CF_3SO_2)_2N$], 0.50 M [C_4C_1Im][$N(CN)_2$], 0.50 M [C_4C_1Im][SCN] (for the last two samples, only the anion fitted components are included; the cation fitted components are not included for clarity). (b) N 1s XPS of nitrogen-containing anions in ionic liquid: [C_8C_1Im][$(FSO_2)_2N$], [C_8C_1Im][$(CF_3SO_2)_2N$], [C_4C_1Im][$N(CN)_2$], [C_8C_1Im][SCN] (for all four samples, only the anion fitted components are included; the cation fitted components are not included for clarity). (c) N 1s XPS of nitrogen-containing anions in propylene carbonate: 0.30 M Na[$(FSO_2)_2N$], 0.14 M Li[$(CF_3SO_2)_2N$], 0.50 M K[SCN]. (d) N 1s XPS of nitrogen-containing anions in triethyl phosphate: 0.50 M Na[$(FSO_2)_2N$], 0.48 M Li[$(CF_3SO_2)_2N$], 0.18 M [C_4C_1Im][SCN] (for the last sample, only the anion fitted component is included; the cation fitted component is not included for clarity). Traces are vertically offset for clarity. Area normalization is to the number of atoms in each anion and explained further in Supporting Information section 8.3. Charge referencing: water $E_B(O_{liquid}\ 1s)$ = 538.13 eV; ionic liquid $E_B(C_{alkyl}\ 1s)$ = 289.85 eV (and $E_B(N_{cation}\ 1s)$ = 406.85 eV for [C_4C_1Im][$N(CN)_2$]); propylene carbonate $E_B(C_{carbonyl}\ 1s)$ = 295.80 eV; triethyl phosphate $E_B(C_{alkyl}\ 1s)$ = 290.32 eV (see Supporting Information section 8.1 and section 8.2 for more details).

different solvent environments (ionic liquids, water, PC, and TEP), e.g., $DN_{O\text{-}XPS}$ calculated in an ionic liquid SMD for $[B(C_2O_4)_2]^-$ can be directly compared to $DN_{O\text{-}XPS}$ measured using ionic liquid experimental XPS (Figure 3 and Table 3). This greatly reduces the need to produce $DN_{E\text{-}XPS}$ from expensive synthesis followed by challenging liquid-phase XPS experiments; the high-vacuum environment required for XPS of ionic liquids and the instability of certain anions under X-ray irradiation, and particularly the need for very challenging and rare synchrotron-based liquid-jet XPS apparatus to study anions in molecular solutions.

For ionic liquids, a high-accuracy and low-cost computational method to predict E_B(core,anion) is already available: lone-anion calculations with a solvation model based on density (SMD), called lone-anion-SMD.[49,73,92,101,113,114] The core-levels included were O 1s, N 1s, F 1s, Cl 2p, and S 2p (and also C 1s and P 2p). To predict E_B(core,anion) and $DN_{E\text{-}XPS}$ in ionic liquids that are comparable to experimental $DN_{E\text{-}XPS}$, a single E_B(correction) is required for the core-level of interest, as long as the same basis set, functional, and SMD parameters are used. The E_B correction for each core-level for ionic liquids is given in Supporting Information Table S11, e.g., +20.69 eV for calculations of $E_B(F_{anion}\ 1s)$; furthermore, eqs S2−S5 can be used to convert uncorrected calculated E_B(core,anion) into $DN_{E\text{-}XPS}$.

E_B(core,anion) and therefore $DN_{E\text{-}XPS}$ can be predicted with high accuracy and low computational cost in molecular solvents for different anions. There are excellent visual matches of experiments and lone-anion-SMD calculations for common anions in water, PC and TEP; both the E_B(core,anion) order and ΔE_B(core,anion) (Figure 7 for water, Supporting Information Figure S68 for PC and TEP). Furthermore, there are excellent linear correlations for calculated E_B(core,anion) against experimental E_B(core,anion); Figure 6b for $E_B(F_{anion}\ 1s)$ and Figure 6d for $E_B(N_{anion}\ 1s)$ for water, Supporting Information Figure S69b,d for PC, Supporting Information Figure S70b,d for TEP. These linear correlations give R^2 near 1 and gradients close to 1. As for calculations of anions in ionic liquid SMD, calculations of anions in water SMD, PC SMD or TEP SMD can accurately and efficiently predict E_B(core,anion) and therefore $DN_{E\text{-}XPS}$ using a single E_B(correction) for each core-level; the E_B corrections for water are given in Supporting Information Table S51, e.g., +20.53 eV for calculations of $E_B(F_{anion}\ 1s)$.

There is great potential for $DN_{E\text{-}XPS}$ as reliable anion descriptors for data-driven discovery, with major advantages over current anion descriptors. First, our $DN_{E\text{-}XPS}$ can be calculated for far more anions than the current experimentally measured (and not cheaply calculated) anion descriptors. Second, calculated $DN_{E\text{-}XPS}$ can be used for fine-tuning anion donor properties (e.g., controlling anion local donor ability by varying R groups on anion families such as $[(RSO_2)_2N]^-$,[115] oxyborate,[27] dicyanoimidazolide[116]). Third, our $DN_{E\text{-}XPS}$ descriptors have the chance to capture the complexity of interactions for anions in the liquid-phase, especially when solvation will be strongly directional/inhomogeneous, e.g., large and complex anions solvating metal cations; our $DN_{E\text{-}XPS}$ descriptors have the potential to give insight into different

https://doi.org/10.1021/jacs.6c06567
J. Am. Chem. Soc. 2026, 148, 35498−35514

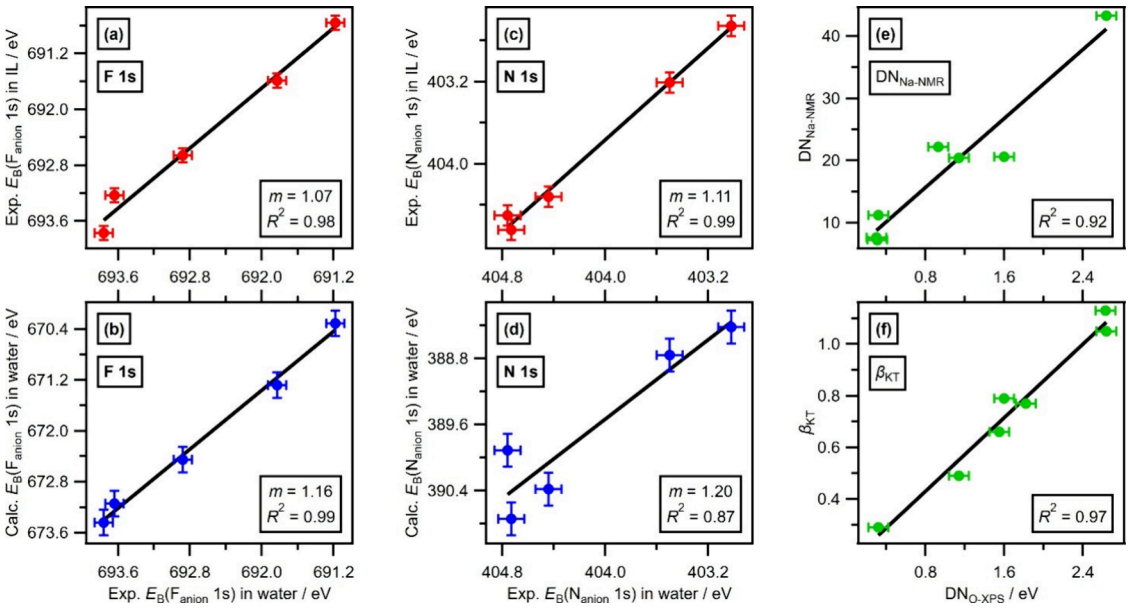

Figure 6. Linear correlations. (a) Experimental $E_B(F_{anion}\ 1s)$ for ionic liquid versus experimental $E_B(F_{anion}\ 1s)$ for water. (b) Calculated $E_B(F_{anion}\ 1s)$ (using lone-anion-SMD for water) versus experimental $E_B(F_{anion}\ 1s)$ in water. (c) Experimental $E_B(N_{anion}\ 1s)$ for ionic liquid versus experimental $E_B(N_{anion}\ 1s)$ for water. (d) Calculated $E_B(N_{anion}\ 1s)$ (using lone-anion-SMD for water) versus experimental $E_B(N_{anion}\ 1s)$ in water. Values used for the linear correlations are given in Table 4, Table 5, Supporting Information Table S39, and Supporting Information Table S40; linear fitting data are given in Supporting Information Table S62. Measures of anion donor ability plotted against $DN_{O\text{-}XPS}$ of $[C_nC_1Im][A]$ neat ionic liquids: (e) anion donor numbers measured from the chemical shift $\delta(Na^+)$ by ^{23}Na NMR spectroscopy of $Na[ClO_4]$ dissolved in $[C_4C_1Im][A]$ neat ionic liquids, $DN_{Na\text{-}NMR}$;[44] (f) Kamlet−Taft hydrogen-bond acceptor numbers using UV−vis spectroscopy comparisons of two different neutral dye molecules in $[C_4C_1Im][A]$ neat ionic liquids, β_{KT}.[51] Six other linear correlations between anion donor ability plotted and $DN_{O\text{-}XPS}$ of $[C_nC_1Im][A]$ neat ionic liquids are given in Supporting Information Figure S71. Values used for the linear correlations are given in Supporting Information Table S63; linear fitting data are given in Supporting Information Table S64. The experimental uncertainty in $DN_{O\text{-}XPS}$ is ±0.10 eV (unless stated otherwise in Supporting Information section 14.2) and calculated uncertainty in $DN_{O\text{-}XPS}$ is ±0.20 eV (Supporting Information section 14.4).

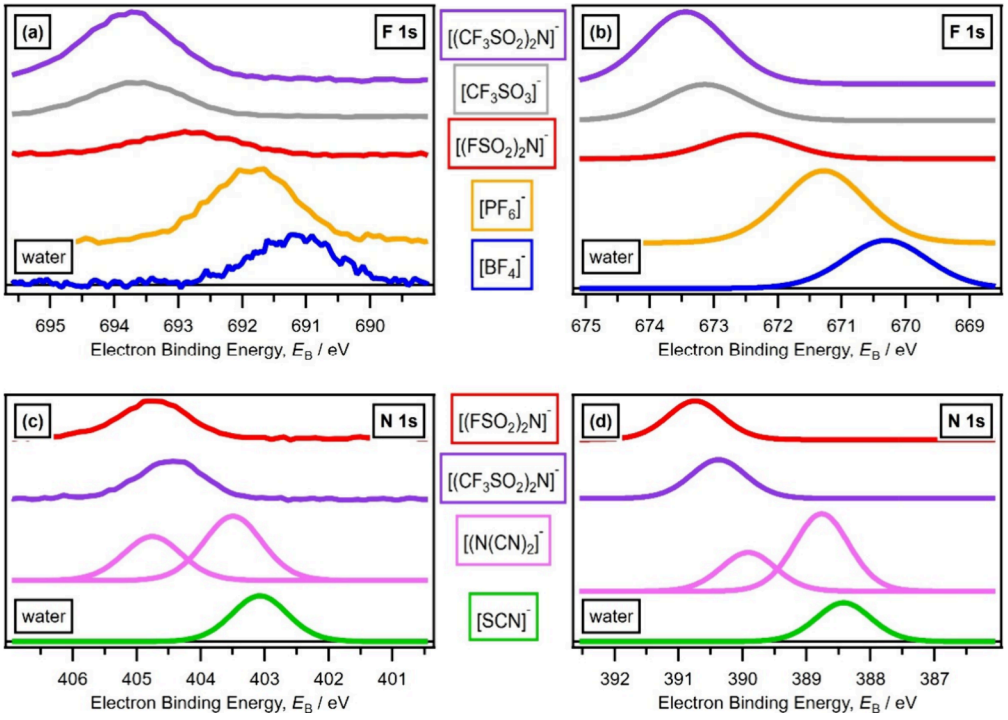

Figure 7. Experimental and calculated XPS spectra for anions. F 1s XP spectra for five different anions: (a) experimental in water (same samples as in Figure 4a,b calculated using lone-anion-SMD for water). N 1s XP spectra for four different anions: (c) experimental in water (same samples as in Figure 5a,d calculated using lone-anion-SMD for water). Traces are vertically offset for clarity. Experimental XPS area normalization is to the number of atoms in each anion and explained further in Supporting Information section 8.1. Calculated XP spectra are produced as explained in Supporting Information section 6. Charge referencing for experimental XP spectra in water $E_B(O_{liquid}\ 1s)$ = 538.13 eV.

https://doi.org/10.1021/jacs.6c06567
J. Am. Chem. Soc. 2026, 148, 35498−35514

anion denticities, unlike current anion-level DN/β descriptors. Fourth, our $DN_{E\text{-}XPS}$ descriptors have great potential as ML training data sets, given that $DN_{E\text{-}XPS}$ can be calculated with high accuracy and low computational cost. Electronic descriptors for molecular solvents have been used as training data for ML,[63] so there is potential for anion descriptors in ML.

The ability of calculated $DN_{E\text{-}XPS}$ to capture the relative donor strength of atoms with different covalent bonding in the same anion is further validated by comparison to interactions in crystal structures. For $[CF_3(C_3N_2)(CN)_2]^-$ (also known as $[TDI]^-$, structure in Figure 1) N_{CN} and N_{ring} have the same $DN_{N\text{-}XPS}$ within calculated uncertainty (Table 4, Supporting Information Figure S57) − we have labeled both N_{CN} and N_{ring} as 1° in Figure 1 and Table 4. This finding matches to crystal structures of $[CF_3(C_3N_2)(CN)_2]^-$ with Li^+, where the shortest Li^+-N_{CN} and Li^+-N_{ring} distances are all within 0.1 Å.[117] For oxygen in $[B(C_2O_4)_2]^-$ (structure in Figure 1), O_{BO} and O_{CO} bonding environments can be readily distinguished in the calculated O 1s XP spectrum (Figure 3, Table 3, structure in Figure 1), with $DN_{O\text{-}XPS}$ larger for O_{CO} than O_{BO}. This finding matches to crystal structures of $[B(C_2O_4)_2]^-$ with Li^+, where the shortest Li^+-O_{CO} distances are ∼1.1 Å shorter than the shortest Li^+-O_{BO} distances.[118]

The intrinsic nature of $DN_{E\text{-}XPS}$ demonstrated in section 2.2 is reinforced by the calculation results presented here in section 2.3. There are no explicit countercations or solvent molecules in lone-anion-SMD calculations, demonstrating that our E_B(core,anion) captures intrinsic differences in anion properties.

2.4. Anion Element-Specific Donor Numbers: Excellent Interpretability

Ground state bonding effects (called initial-state effects in the XPS community) dominate ΔE_B(core,anion), and therefore $DN_{E\text{-}XPS}$, measured in the same solvent, as conclusively demonstrated by the linear correlations between experimental and calculated E_B(core,anion) for all solvents studied here (see section 2.3 and references[49,73,92,101,113,114]). The influence of the core-hole created during photoemission (final-state effects) on ΔE_B(core,anion) is minimal.

E_B(core,anion), and therefore $DN_{E\text{-}XPS}$, is a measure of donor ability, based on a number of excellent correlations presented here between: (i) experimental E_B(core,anion) for ionic liquids and experimental E_B(core,anion) for molecular solvents (section 2.2); (ii) experimental E_B(core,anion) and calculated E_B(core,anion) for ionic liquids (section 2.3 and references[73,92,101]); (iii) experimental E_B(core,anion) and calculated E_B(core,anion) for water, PC and TEP (section 2.3); (iv) experimental and calculated E_B(core,anion) and calculated V_n for ionic liquids;[49,101,113] (v) V_n and donor ability.[119−121] We can also conclude with high confidence that $\Delta DN_{E\text{-}XPS}$ will capture ΔV_n(anion) and therefore anion donor ability for anions solvated by other solvents used for battery electrolytes (e.g., carbonate mixtures, acetonitrile), as the solvents we have studied cover an excellent range of solvent properties.

Our results are excellent experimental evidence that the calculated ESP, closely related to V_n, can be used to judge the local donor ability. We are unaware of any study using calculated ESP to help select anions for batteries. However, calculated ESP descriptors are a recent and growing area in the battery community, to identify which part of the molecule has good electron donor ability,[63,64] and capturing oxygen atom donor strength.[68]

We make a recommendation here with regard to placing the location of the negative charge on a chemical structure of an anion. Many researchers may have given this point little thought. However, such placement can be misleading, e.g., placing the negative charge near the central N_{CNC} in $[N(CN)_2]^-$, near N_{ring} in $[CF_3(C_3N_2)(CN)_2]^-$ (structure in Figure 1). Hence, in this article, all negative charge symbols are represented over the whole anion in each case (e.g., Figure 1), and we recommend this as a general approach for all anion chemical structures to avoid misinterpretation.

There is a trade-off when using $DN_{E\text{-}XPS}$ compared to existing experimental (single value and probe-dependent) anion descriptors; significant atomic-level insight is gained, but overall comparability across all anions is decreased. $DN_{E\text{-}XPS}$ provide more than one descriptor for many anions and can be applied to all anions; one just needs two (or more) anions containing a particular element to construct a $DN_{E\text{-}XPS}$ descriptor. However, a single $DN_{E\text{-}XPS}$ descriptor is not presented here that covers all anions; not all anions contain, for example, oxygen. In the future, we will attempt to produce a single descriptor that brings together $DN_{E\text{-}XPS}$ for the different elements. We know that $\Delta E_B(O_{anion}\ 1s) = 1$ eV and $\Delta E_B(F_{anion}\ 1s) = 1$ eV correspond to $\Delta V_O \approx 1$ eV and $\Delta V_F \approx 1$ eV respectively. The question then arises: Does $\Delta V_O = 1$ eV represent the same change in donor ability as $\Delta V_F = 1$ eV? From our literature searches it appears that V_n values are only ever compared for the same element,[119−121] so this question has not yet been rigorously answered, suggesting that obtaining a single anion descriptor from E_B(core,anion) is still some way off.

2.5. Fine-Tuning $DN_{E\text{-}XPS}$ for $[(RSO_2)_2N]^-$: Implications for Battery Electrolyte Selection

The effect on $[(RSO_2)_2N]^-$ donor ability of decreased fluorination from R = CF_3 to R = F is relatively large; this can potentially impact battery electrolyte performance, e.g., in lithium-ion batteries. First, changing from R = CF_3 to R = F can potentially improve battery stability due to increased chances of LiF formation at the SEI,[35,36] caused by (a) much larger $DN_{F\text{-}XPS}$ (Figure 8a) and therefore stronger 3° Li^+−F interactions; (b) smaller $DN_{N\text{-}XPS}$ (Figure 8b) and therefore weaker 2° Li^+-N interactions. Second, changing from R = CF_3 to R = F likely reduces the Li^+-anion desolvation energy at the SEI through an improvement in this potentially rate-determining step in battery charging, caused by smaller $DN_{O\text{-}XPS}$ (Figure 8c) and therefore weaker 1° Li^+−O interactions. Lastly, changing from R = CF_3 to R = F will lead to weaker transition metal-N interactions from smaller $DN_{N\text{-}XPS}$ (Figure 8b) when metal dissolution from the cathode occurs,[122] as N can become the 1° donor atom for $[(RSO_2)_2N]^-$.[105]

The effect on the $[(RSO_2)_2N]^-$ donor ability of increased fluorination from R = CF_3 to R = C_2F_5 is minimal. Altering R = CF_3 to R = C_2F_5 leads to no change within experimental uncertainty of $DN_{N\text{-}XPS}$ (Figure 8b) or $DN_{O\text{-}XPS}$ (Figure 8c). Therefore, changing from R = CF_3 to C_2F_5 will provide little difference in Li^+−O or Li^+−N interaction strengths. There is a suggestion from $DN_{F\text{-}XPS}$ that increasing fluorination leads to slightly smaller $DN_{F\text{-}XPS}$ and therefore slightly weaker Li^+-F interactions (experimental data in Figure 8a and calculated $E_B(F_{anion}\ 1s)$ in ref[73]); of course, increasing fluorination may

https://doi.org/10.1021/jacs.6c06567
J. Am. Chem. Soc. 2026, 148, 35498−35514

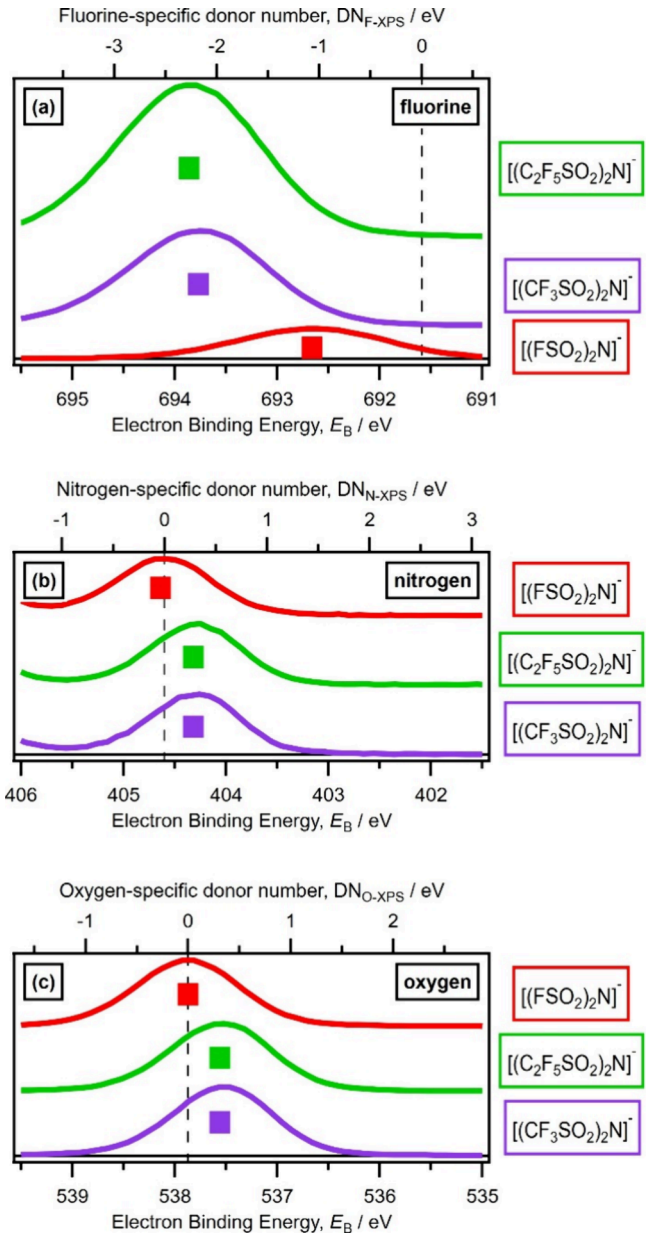

Figure 8. Values of E_B(core,anion) and DN$_{E-XPS}$ (bottom and top axes, respectively) for the three ionic liquids $[C_8C_1Im][(FSO_2)_2N]$, $[C_4C_1Im][(C_2F_5SO_2)_2N]$, and $[C_8C_1Im][(CF_3SO_2)_2N]$: (a) O 1s, (b) N 1s, (c) F 1s. Values are vertically offset for clarity. Charge referencing is given in Supporting Information section 8.2. For E_B(core,anion) (and therefore DN$_{E-XPS}$), the experimental uncertainty is ±0.10 eV (Supporting Information section 14.2); these uncertainty values are represented by the width of each block.

also lead to an increase in the number of Li^+−F interactions given the greater number of F atoms in the anion, so overall any effect is likely to be minimal.

3. CONCLUSIONS AND FUTURE WORK

Robust and interpretable new element-specific donor number descriptors, DN$_{E-XPS}$, are defined and measured using a combination of experimental XPS and low-cost, simple calculations. New methods for producing DNs are rarely discovered; DN$_{E-XPS}$ greatly expands and enhances the small toolbox of existing DN descriptors.

DN$_{E-XPS}$ descriptors capture local (i.e., atomic level) atom donor abilities. We provide separate anion DN$_{E-XPS}$ for seven different elements (O, N, F, Cl, Br, I, S); each anion 1°, 2°, and 3° donor atom has its own DN$_{E-XPS}$ value. DN$_{E-XPS}$ can be used to evaluate anion-substrate interactions by 2° and 3° anion donor atoms, unlike anion-level descriptors, providing insight into rare reactivity events. For example, for battery electrolyte selection DN$_{O-XPS}$, DN$_{N-XPS}$ and DN$_{F-XPS}$ can be used to predict that $[(FSO_2)_2N]^-$ will provide superior electrolyte performance over $[(CF_3SO_2)_2N]^-$ and $[(C_2F_5SO_2)_2N]^-$ with regard to both anion−metal cation desolvation and LiF formation at the SEI.

DN$_{E-XPS}$ can be applied with confidence to a wide range of anion−substrate interactions, as DN$_{E-XPS}$ captures intrinsic anion donor ability, independent of specific probe cation/molecule interactions. Furthermore, there is the potential to gain molecular-level insight into anion interactions by comparing DN$_{E-XPS}$ against other descriptors; however, more experimental data are required for existing anion descriptors to make the most of this opportunity.

DN$_{E-XPS}$ can be used for data-driven discovery. The cheap and low-cost calculation method for DN$_{E-XPS}$ presented here, in conjunction with our substantial existing DN$_{E-XPS}$ database for anions, opens up the possibility of using DN$_{E-XPS}$ for both fine-tuning anion donor properties (e.g., controlling anion local donor ability by varying R groups on anion families such as $[(RSO_2)_2N]^-$,[115] oxyborate,[27] dicyanoimidazolide[116]) and as anion descriptors for machine learning (ML) training data sets.

The development of a full picture of liquid-phase donor ability for both anions and molecules, which would fast-forward data-driven discovery, is a long-term goal. DN$_{E-XPS}$ scales including both anions and molecules (i.e., solvents/additives) for each element are needed, extending beyond the DN$_{E-XPS}$ scales for anions published here.

4. METHODS

4.1. Samples Studied and Preparation

44 anions are studied (44 $[C_nC_1Im][anion]$ ionic liquids in total) using a combination of literature and new data (Supporting Information Table S5); seven ionic liquids were measured on multiple apparatuses to demonstrate the small experimental uncertainty (Supporting Information section 14.2). All XPS data for anions in molecular solvents are new here: seven anions in water (15 samples, Supporting Information Table S6); five anions in PC (nine samples, Supporting Information Table S7); and four anions in TEP (five samples, Supporting Information Table S8).

Lone-anion SMD (ionic liquid) calculations were carried out for four new anions; results from these calculations are used in conjunction with previously published calculations for three anions from ref 123 (Table S9). Lone-anion SMD (water) calculations were carried out for nine new anions (Table S9).

4.2. Experimental Apparatus

4.2.1. Ionic Liquid Drop XPS Apparatus. Laboratory-based XPS measurements for two ionic liquid samples were performed at the University of Reading on a Thermo Scientific ESCALAB 250 monochromated Al Kα source ($h\nu$ = 1486.6 eV) spectrometer and for one ionic liquid sample was performed at University College London on a Thermo Scientific Theta Probe monochromated Al Kα source ($h\nu$ = 1486.6 eV) spectrometer. A drop of ionic liquid was placed directly onto a stainless steel sample plate. XPS apparatus used for literature E_B(core,anion) has already been described elsewhere.[48,49,73,86,91−95,124,125]

Synchrotron-based XPS measurements for nine ionic liquid samples were performed at beamline B07-B XPS.[114,126] A drop of

https://doi.org/10.1021/jacs.6c06567
J. Am. Chem. Soc. 2026, 148, 35498−35514

ionic liquid was placed directly onto a custom-made tantalum sample plate. Rastering of the sample was performed to minimize sample charging/damage.

4.2.2. Liquid-Jet XPS Apparatus. Solutes were weighed and mixed with a corresponding mass of the solvent to achieve the desired concentration. A liquid-jet apparatus was used. The measurement for eight solutions was performed on the U49/2-PGM 1 beamline with SOL^{3}PES end-station[127] at the BESSY II electron storage ring (Germany). XP spectra were acquired using a Scienta Omicron R4000 HIPP-2 hemispherical electron analyzer. The measurement for 16 solutions was performed on the HIPPIE beamline[128] at the MAX IV II electron storage ring (Sweden). XP spectra were acquired using the Solid–Liquid Endstation with a SPECS Phoibos 150 hemispherical electron analyzer. The measurement for five solutions was performed on the GALAXIES beamline[129] at the Soleil electron storage ring (France). XP spectra were acquired by using an EW4000 hemispherical electron analyzer.

4.3. Calculations

All DFT calculations were carried out using Gaussian 16 (version C.01).[130] Each of the anions was optimized under no symmetry constraints and confirmed as a minimum using vibrational analysis. DFT calculations were carried out at the B3LYP-D3(BJ)/6-311+G-(d,p) level. The SMD (solvation model based on density) was employed to account for solvation effects. Specifically, the $[C_4C_1Im]$-$[PF_6]$ parameters (Supporting Information Table S10) were selected to be consistent with previous ionic liquid work.[92] The SMD solvent continua for water, PC and TEP (Supporting Information Table S10) were also employed. Optimization convergence criteria were set to 10^{-11} on the density matrix and 10^{-9} on the energy matrix. Moreover, the numerical grid was improved from the default using the "int=ultrafine" keyword. Vibrational frequencies and zero-point vibrational energy corrections (ZPE) were attained using the harmonic approximation.

4.4. Data Analysis

4.4.1. Component Fitting for Core-Level XPS. All experimental XP spectra were fitted using CASAXPS software.[131] Fitting was carried out using a Shirley/linear background and GL30 line shapes (70% Gaussian, 30% Lorentzian). Peak constraints used are outlined in Supporting Information Tables S13–S16. Relative sensitivity factors (RSFs) from ref 132 were used for XPS recorded at $h\nu$ = 1486.6 eV to ensure the experimental stoichiometries matched the nominal stoichiometries (Supporting Information Table S21, Supporting Information section 10).

4.4.2. Charge Referencing. Each sample was internally charge referenced, effectively to the vacuum level. Each of the three molecular solvent systems studied here (water, PC, TEP) were charge referenced to a single solvent-specific core-level (Supporting Information section 8.1): water $E_B(O_{liquid}\ 1s)$ = 538.13 eV; propylene carbonate $E_B(C_{carbonyl}\ 1s)$ = 295.80 eV; triethyl phosphate $E_B(C_{alkyl}\ 1s)$ = 290.32 eV (Supporting Information Tables S17 to S19). For ionic liquids, we used an adaptation of the very well-established method for charge referencing ionic liquid XPS (Supporting Information Table S20).[49,73,84] It is common practice for ionic liquid XPS to charge reference E_B(core) effectively to the Fermi level using either $E_B(C_{alkyl}\ 1s)$ = 285.00 eV for ionic liquids with long alkyl chains or an anion-specific $E_B(N_{cation}\ 1s)$ value for ionic liquids with shorter alkyl chains.[125] Here we charge reference ionic liquid XPS to the vacuum level to match the charge referencing level used for anions in molecular solvents by adding 4.85 eV to E_B(core) values charge-referenced to the Fermi level (the 4.85 eV value can be thought of as a work function value). E_B(core) values used for charge referencing ionic liquid XPS are given in Supporting Information section 8.2, e.g., $E_B(C_{alkyl}\ 1s)$ = 289.85 eV for $[C_8C_1Im][anion]$ ionic liquids (Supporting Information Table S20).

■ ASSOCIATED CONTENT

Data Availability Statement

The data underlying this study are openly available in the University of Bath Research Data Archive at https://doi.org/10.15125/BATH-01706.

Supporting Information

The Supporting Information is available free of charge at https://pubs.acs.org/doi/10.1021/jacs.6c06567.

Methods (samples studied, calculation method, how to produce calculated and "experimental" XP spectra); data analysis (peak fitting, charge referencing, producing $DN_{E\text{-}XPS}$); results (demonstrating purity, uncertainty, E_B(core,anion) values, effect of countercations on $DN_{E\text{-}XPS}$, linear correlations and bulk versus surface contributions) (PDF)

■ AUTHOR INFORMATION

Corresponding Author

Kevin R. J. Lovelock − *Department of Chemistry, University of Reading, Reading RG6 6DX, U.K.; Department of Chemistry, University of Bath, Bath BA2 7AY, U.K.;* orcid.org/0000-0003-1431-269X; Email: krjl20@bath.ac.uk

Authors

Lewis G. Parker − *Department of Chemistry, University of Reading, Reading RG6 6DX, U.K.; Department of Chemistry, University of Bath, Bath BA2 7AY, U.K.*

Frances K. Towers Tompkins − *Department of Chemistry, University of Reading, Reading RG6 6DX, U.K.*

Jake M. Seymour − *Department of Chemistry, University of Reading, Reading RG6 6DX, U.K.*

Ekaterina Gousseva − *Department of Chemistry, University of Reading, Reading RG6 6DX, U.K.*

Christopher D. Smith − *Department of Chemistry, University of Reading, Reading RG6 6DX, U.K.*

Roger A. Bennett − *Department of Chemistry, University of Reading, Reading RG6 6DX, U.K.;* orcid.org/0000-0001-6266-3510

Pilar Ferrer − *Diamond Light Source, Didcot, Oxfordshire OX11 0DE, U.K.;* orcid.org/0000-0001-9807-7679

David C. Grinter − *Diamond Light Source, Didcot, Oxfordshire OX11 0DE, U.K.;* orcid.org/0000-0001-6089-119X

Claudia Kolbeck − *Fritz-Haber-Institut der Max-Planck-Gesellschaft, 14195 Berlin, Germany*

Dennis Hein − *Helmholtz-Zentrum Berlin für Materialien und Energie GmbH, 14109 Berlin, Germany*

Garlef Wartner − *Helmholtz-Zentrum Berlin für Materialien und Energie GmbH, 14109 Berlin, Germany*

Robert Seidel − *Helmholtz-Zentrum Berlin für Materialien und Energie GmbH, 14109 Berlin, Germany;* orcid.org/0000-0003-2613-4106

Denis Céolin − *Synchrotron SOLEIL, 91192 Gif sur Yvette, France;* orcid.org/0000-0002-5660-137X

Robert Temperton − *MAX IV Laboratory, Lund University, 221 00 Lund, Sweden;* orcid.org/0000-0002-4802-6862

Robert G. Palgrave − *Department of Chemistry, University College London, London WC1H 0AJ, U.K.;* orcid.org/0000-0003-4522-2486

Richard P. Matthews − *School of Health, Sport and Bioscience, University of East London, London E15 4LZ, U.K.;* orcid.org/0000-0003-3328-4954

Complete contact information is available at: https://pubs.acs.org/10.1021/jacs.6c06567

Notes

The authors declare no competing financial interest.

■ ACKNOWLEDGMENTS

This work was carried out with the support of Diamond Light Source, instrument B07-B-XPS (Proposals SI33378, SI35207, SI36765, SI36196). We thank the Helmholtz-Zentrum Berlin für Materialien und Energie for the allocation of synchrotron radiation beamtime on beamline UG49/2, SOL^{3}PES end-station (experiment 181-06684-ST-1, 182-07370-ST-1, 192-08760-ST, 212-10428-ST). The research leading to this result has been supported by the project CALIPSOplus under Grant Agreement 730872 from the EU Framework Programme for Research and Innovation HORIZON 2020. We acknowledge the MAX IV Laboratory for beamtime on the HIPPIE beamline under Proposals 20220324, 20230605, 20240694, 20241911, 20251059. Research conducted at MAX IV, a Swedish national user facility, is supported by Vetenskapsrådet (Swedish Research Council, VR) under Contract 2018-07152, Vinnova (Swedish Governmental Agency for Innovation Systems) under Contract 2018-04969, and Formas under Contract 2019-02496. We acknowledge SOLEIL for provision of synchrotron radiation facilities (beamline GALAXIES under Proposals 20190203, 20200483, 20210460, 20220667, 20240614). K.R.J.L. acknowledges support from a Royal Society University Research Fellowship (URF\R\150353 and URF\R\211005).

■ REFERENCES

(1) Huang, Z.; Li, X.; Chen, Z.; Li, P.; Ji, X.; Zhi, C. Anion chemistry in energy storage devices. *Nat. Rev. Chem.* **2023**, *7*, 616−631.
(2) MacFarlane, D. R.; Forsyth, M.; Howlett, P. C.; Kar, M.; Passerini, S.; Pringle, J. M.; Ohno, H.; Watanabe, M.; Yan, F.; Zheng, W. J.; Zhang, S. G.; Zhang, J. Ionic liquids and their solid-state analogues as materials for energy generation and storage. *Nat. Rev. Mater.* **2016**, *1*, No. 15005.
(3) Wang, Z. X.; Sun, Z. H.; Li, J.; Shi, Y.; Sun, C. G.; An, B. G.; Cheng, H. M.; Li, F. Insights into the deposition chemistry of Li ions in nonaqueous electrolyte for stable Li anodes. *Chem. Soc. Rev.* **2021**, *50*, 3178−3210.
(4) Holoubek, J.; Liu, H. D.; Wu, Z. H.; Yin, Y. J.; Xing, X.; Cai, G. R.; Yu, S. C.; Zhou, H. Y.; Pascal, T. A.; Chen, Z.; Liu, P. Tailoring electrolyte solvation for Li metal batteries cycled at ultra-low temperature. *Nat. Energy* **2021**, *6*, 303−313.
(5) Lu, Z.; Geng, C.; Yang, H.; He, P.; Wu, S.; Yang, Q.; Zhou, H. Step-by-step desolvation enables high-rate and ultra-stable sodium storage in hard carbon anodes. *Proc. Natl. Acad. Sci. U. S. A.* **2022**, *119*, 9.
(6) Han, J.; Mariani, A.; Passerini, S.; Varzi, A. A perspective on the role of anions in highly concentrated aqueous electrolytes. *Energy Environ. Sci.* **2023**, *16*, 1480−1501.
(7) Xiao, Y.; Xu, R.; Xu, L.; Ding, J. F.; Huang, J. Q. Recent advances in anion-derived SEIs for fast- charging and stable lithium batteries. *Energy Mater.* **2022**, *1*, No. 100013.
(8) Li, T.; Zhang, X. Q.; Yao, N.; Yao, Y. X.; Hou, L. P.; Chen, X.; Zhou, M. Y.; Huang, J. Q.; Zhang, Q. Stable Anion-Derived Solid Electrolyte Interphase in Lithium Metal Batteries. *Angew. Chem., Int. Ed.* **2021**, *60*, 22683−22687.
(9) Park, G.; Lee, K.; Yoo, D. J.; Choi, J. W. Strategy for Stable Interface in Lithium Metal Batteries: Free Solvent Derived vs Anion Derived. *ACS Energy Lett.* **2022**, *7*, 4274−4281.
(10) Schroder, K. W.; Dylla, A. G.; Bishop, L. D. C.; Kamilar, E. R.; Saunders, J.; Webb, L. J.; Stevenson, K. J. Effects of Solute-Solvent Hydrogen Bonding on Nonaqueous Electrolyte Structure. *J. Phys. Chem. Lett.* **2015**, *6*, 2888−2891.
(11) Yamada, Y.; Usui, K.; Chiang, C. H.; Kikuchi, K.; Furukawa, K.; Yamada, A. General Observation of Lithium Intercalation into Graphite in Ethylene-Carbonate-Free Superconcentrated Electrolytes. *ACS Appl. Mater. Interfaces* **2014**, *6*, 10892−10899.
(12) Chen, X.; Zhang, Q. Atomic Insights into the Fundamental Interactions in Lithium Battery Electrolytes. *Acc. Chem. Res.* **2020**, *53*, 1992−2002.
(13) Brandt, A.; Gräsvik, J.; Hallett, J. P.; Welton, T. Deconstruction of lignocellulosic biomass with ionic liquids. *Green Chem.* **2013**, *15*, 550−583.
(14) Du, H.; Chatti, M.; Hodgetts, R.; Cherepanov, P.; Nguyen, C.; Matuszek, K.; MacFarlane, D.; Simonov, A. Electroreduction of nitrogen with almost 100% current-to-ammonia efficiency. *Nature* **2022**, *609*, 722−727.
(15) Estager, J.; Holbrey, J. D.; Swadźba-Kwaśny, M. Halometallate ionic liquids - revisited. *Chem. Soc. Rev.* **2014**, *43*, 847−886.
(16) Riddlestone, I. M.; Kraft, A.; Schaefer, J.; Krossing, I. Taming the Cationic Beast: Novel Developments in the Synthesis and Application of Weakly Coordinating Anions. *Angew. Chem., Int. Ed.* **2018**, *57*, 13982−14024.
(17) Brak, K.; Jacobsen, E. Asymmetric Ion-Pairing Catalysis. *Angew. Chem., Int. Ed.* **2013**, *52*, 534−561.
(18) Ovian, J.; Vojácková, P.; Jacobsen, E. Enantioselective transition-metal catalysis via an anion-binding approach. *Nature* **2023**, *616*, 84−89.
(19) Noh, J.; Kim, H.; Park, H.; Chung, D. The Roles of Ions in Electrochemical Interface for Electrocatalysis. *ACS Catal.* **2025**, *15*, 7780−7791.
(20) Yoo, J.; Ingenmey, J.; Salanne, M.; Lukatskaya, M. Anion Effect in Electrochemical CO2 Reduction: From Spectators to Orchestrators. *J. Am. Chem. Soc.* **2024**, *146*, 31768−31777.
(21) Jungwirth, P.; Cremer, P. S. Beyond Hofmeister. *Nat. Chem.* **2014**, *6*, 261−263.
(22) Okur, H.; Hladílková, J.; Rembert, K.; Cho, Y.; Heyda, J.; Dzubiella, J.; Cremer, P.; Jungwirth, P. Beyond the Hofmeister Series: Ion-Specific Effects on Proteins and Their Biological Functions. *J. Phys. Chem. B* **2017**, *121*, 1997−2014.
(23) Xia, Y.; Zhou, P.; Kong, X.; Tian, J.; Zhang, W.; Yan, S.; Hou, W.; Zhou, H.; Dong, H.; Chen, X.; Wang, P.; Xu, Z.; Wan, L.; Wang, B.; Liu, K. Designing an asymmetric ether-like lithium salt to enable fast-cycling high-energy lithium metal batteries. *Nat. Energy* **2023**, *8*, 934−945.
(24) Min, X.; Han, C.; Zhang, S.; Ma, J.; Hu, N.; Li, J.; Du, X.; Xie, B.; Lin, H.; Kuo, C.; Chen, C.; Hu, Z.; Qiao, L.; Cui, Z.; Xu, G.; Cui, G. Highly Oxidative-Resistant Cyano-Functionalized Lithium Borate Salt for Enhanced Cycling Performance of Practical Lithium-Ion Batteries. *Angew. Chem., Int. Ed.* **2023**, *62*, 8.
(25) Song, Z. Y.; Wang, X. X.; Feng, W. F.; Armand, M.; Zhou, Z. B.; Zhang, H. Designer Anions for Better Rechargeable Lithium Batteries and Beyond. *Adv. Mater.* **2024**, *36*, 49.
(26) Lu, Y.; Cao, Q.; Zhang, W.; Zeng, T.; Ou, Y.; Yan, S.; Liu, H.; Song, X.; Zhou, H.; Hou, W.; Zhou, P.; Hu, N.; Feng, Q.; Li, Y.; Liu, K. Breaking the molecular symmetricity of sulfonimide anions for high-performance lithium metal batteries under extreme cycling conditions. *Nat. Energy* **2024**, *10*, 191−204.
(27) Ould, D.; Ruff, Z.; Penrod, M.; Didwal, P.; Weiss, T.; Mylrea, K.; Smith, H.; Bond, A.; Weatherup, R.; Grey, C.; Wright, D. Synthesis and Electrolyte Study of Lithium Bis(perfluorinated pinacolato)Borate for Lithium-Ion Batteries. *Chem.—Eur. J.* **2025**, *31*, 10.
(28) Wu, Y.; Wang, H.; Goh, S.; Chen, J.; Ma, X.; Lu, Y.; Zhou, P.; Yan, S.; Xia, Y.; Liu, Z.; Hou, W.; Ou, Y.; Zhang, Y.; Li, C.; Song, X.;

Wei, L.; Li, K.; Liu, K. Rational Design of Asymmetric Lithium Salts with Multi-Functional Capabilities for Stable Lithium Metal Batteries. *Angew. Chem., Int. Ed.* **2026**, *65*, 13.
(29) Yanai, H. Stable and isolable carbanions: synthesis, chemical bonding, and unique applications. *Coord. Chem. Rev.* **2026**, *554*, 217522.
(30) Han, S. D.; Yun, S. H.; Borodin, O.; Seo, D. M.; Sommer, R. D.; Young, V. G.; Henderson, W. A. Solvate Structures and Computational/Spectroscopic Characterization of $LiPF_6$ Electrolytes. *J. Phys. Chem. C* **2015**, *119*, 8492−8500.
(31) Chapman, N.; Borodin, O.; Yoon, T.; Nguyen, C. C.; Lucht, B. L. Spectroscopic and Density Functional Theory Characterization of Common Lithium Salt Solvates in Carbonate Electrolytes for Lithium Batteries. *J. Phys. Chem. C* **2017**, *121*, 2135−2148.
(32) Takeuchi, M.; Kameda, Y.; Umebayashi, Y.; Ogawa, S.; Sonoda, T.; Ishiguro, S. I.; Fujita, M.; Sano, M. Ion-ion interactions of $LiPF_6$ and $LiBF_4$ in propylene carbonate solutions. *J. Mol. Liq.* **2009**, *148*, 99−108.
(33) Takeuchi, M.; Matubayasi, N.; Kameda, Y.; Minofar, B.; Ishiguro, S.; Umebayashi, Y. Free-Energy and Structural Analysis of Ion Solvation and Contact Ion-Pair Formation of Li⁺ with BF_4 ⁻ and PF_6 ⁻ in Water and Carbonate Solvents. *J. Phys. Chem. B* **2012**, *116*, 6476−6487.
(34) Mennucci, B.; Cances, E.; Tomasi, J. Evaluation of solvent effects in isotropic and anisotropic dielectrics and in ionic solutions with a unified integral equation method: Theoretical bases, computational implementation, and numerical applications. *J. Phys. Chem. B* **1997**, *101*, 10506−10517.
(35) Borodin, O.; Giffin, G. A.; Moretti, A.; Haskins, J. B.; Lawson, J. W.; Henderson, W. A.; Passerini, S. Insights into the Structure and Transport of the Lithium, Sodium, Magnesium, and Zinc Bis-(trifluoromethansulfonyl)imide Salts in Ionic Liquids. *J. Phys. Chem. C* **2018**, *122*, 20108−20121.
(36) Zhang, X. Q.; Chen, X.; Hou, L. P.; Li, B. Q.; Cheng, X. B.; Huang, J. Q.; Zhang, Q. Regulating Anions in the Solvation Sheath of Lithium Ions for Stable Lithium Metal Batteries. *ACS Energy Lett.* **2019**, *4*, 411−416.
(37) Cui, B. C.; Xu, J. J. Enabling rational electrolyte design for lithium batteries through precise descriptors: progress and future perspectives. *J. Mater. Chem. A* **2025**, *13*, 8223.
(38) Gao, Y. C.; Yao, N.; Chen, X.; Yu, L. G.; Zhang, R.; Zhang, Q. Data-Driven Insight into the Reductive Stability of Ion-Solvent Complexes in Lithium Battery Electrolytes. *J. Am. Chem. Soc.* **2023**, *145*, 23764−23770.
(39) Fichtner, M.; Edström, K.; Ayerbe, E.; Berecibar, M.; Bhowmik, A.; Castelli, I. E.; Clark, S.; Dominko, R.; Erakca, M.; Franco, A. A.; Grimaud, A.; Horstmann, B.; Latz, A.; Lorrmann, H.; Meeus, M.; Narayan, R.; Pammer, F.; Ruhland, J.; Stein, H.; Vegge, T.; Weil, M. Rechargeable Batteries of the Future-The State of the Art from a BATTERY 2030+Perspective. *Adv. Energy Mater.* **2022**, *12*, No. 2102904.
(40) Lv, C. D.; Zhou, X.; Zhong, L. X.; Yan, C. S.; Srinivasan, M.; Seh, Z. W.; Liu, C. T.; Pan, H. G.; Li, S. Z.; Wen, Y. G.; Yan, Q. Y. Machine Learning: An Advanced Platform for Materials Development and State Prediction in Lithium-Ion Batteries. *Adv. Mater.* **2022**, *34*, No. 2101474.
(41) Nair, M. R.; Roy, T. Role of artificial intelligence in the design and discovery of next-generation battery electrolytes. *Chem. Phys. Rev.* **2025**, *6*, No. 011311.
(42) Deng, J.; Chen, X.; Bai, Y.; Mo, J.; Yu, X. Data-Driven Electrolyte Design for Advanced Rechargeable Lithium Batteries. *Chin. J. Chem.* **2026**, *44*, 403.
(43) Zhou, P.; Xiang, Y.; Liu, K. Understanding and applying the donor number of electrolytes in lithium metal batteries. *Energy Environ. Sci.* **2024**, *17*, 8057−8077.
(44) Schmeisser, M.; Illner, P.; Puchta, R.; Zahl, A.; van Eldik, R. Gutmann Donor and Acceptor Numbers for Ionic Liquids. *Chem.—Eur. J.* **2012**, *18*, 10969−10982.
(45) Kulkarni, U.; Cho, W. J.; Lee, S. H. Y.; Hwang, D. S.; Im, T.; Jeong, Y. K.; Ahn, K.; Yi, G. R. Donor Numbers for Ionic Liquids and Carbonate Solvents Using ⁷Li and ²³Na as Probes. *Korean J. Chem. Eng.* **2025**, *42*, 225−231.
(46) Holzweber, M.; Lungwitz, R.; Doerfler, D.; Spange, S.; Koel, M.; Hutter, H.; Linert, W. Mutual Lewis Acid-Base Interactions of Cations and Anions in Ionic Liquids. *Chem.—Eur. J.* **2013**, *19*, 288−293.
(47) Lungwitz, R.; Spange, S. A hydrogen bond accepting (HBA) scale for anions, including room temperature ionic liquids. *New J. Chem.* **2008**, *32*, 392−394.
(48) Cremer, T.; Kolbeck, C.; Lovelock, K. R. J.; Paape, N.; Wölfel, R.; Schulz, P. S.; Wasserscheid, P.; Weber, H.; Thar, J.; Kirchner, B.; Maier, F.; Steinrück, H. P. Towards a Molecular Understanding of Cation-Anion Interactions-Probing the Electronic Structure of Imidazolium Ionic Liquids by NMR Spectroscopy, X-ray Photoelectron Spectroscopy and Theoretical Calculations. *Chem.—Eur. J.* **2010**, *16*, 9018−9033.
(49) Gousseva, E.; Towers Tompkins, F. K.; Seymour, J. M.; Parker, L. G.; Clarke, C. J.; Palgrave, R. G.; Bennett, R. A.; Grau-Crespo, R.; Lovelock, K. R. J. Anion-Dependent Strength Scale of Interactions in Ionic Liquids from X-ray Photoelectron Spectroscopy, Ab Initio Molecular Dynamics, and Density Functional Theory. *J. Phys. Chem. B* **2024**, *128*, 5030−5043.
(50) Spange, S.; Lungwitz, R.; Schade, A. Correlation of molecular structure and polarity of ionic liquids. *J. Mol. Liq.* **2014**, *192*, 137−143.
(51) Ab Rani, M. A.; Brant, A.; Crowhurst, L.; Dolan, A.; Hassan, N. H.; Hallett, J. P.; Hunt, P. A.; Lui, M.; Niedermeyer, H.; Perez-Arlandis, J. M.; Schrems, M.; To, T. Q.; Welton, T.; Wilding, R. Understanding the polarity of ionic liquids. *Phys. Chem. Chem. Phys.* **2011**, *13*, 16831−16840.
(52) Laurence, C.; Mansour, S.; Vuluga, D.; Legros, J. Measurement of the hydrogen bond acceptance of ionic liquids and green solvents by the F-19 solvatomagnetic comparison method. *Green Chem.* **2021**, *23*, 1816−1822.
(53) Pike, S. J.; Hutchinson, J. J.; Hunter, C. A. H-Bond Acceptor Parameters for Anions. *J. Am. Chem. Soc.* **2017**, *139*, 6700−6706.
(54) Burke, C. M.; Pande, V.; Khetan, A.; Viswanathan, V.; McCloskey, B. D. Enhancing electrochemical intermediate solvation through electrolyte anion selection to increase nonaqueous Li-O-2 battery capacity. *Proc. Natl. Acad. Sci. U. S. A.* **2015**, *112*, 9293−9298.
(55) Chu, H.; Jung, J.; Noh, H.; Yuk, S.; Lee, J.; Lee, J. H.; Baek, J.; Roh, Y.; Kwon, H.; Choi, D.; Sohn, K.; Kim, Y.; Kim, H. T. Unraveling the Dual Functionality of High-Donor-Number Anion in Lean-Electrolyte Lithium-Sulfur Batteries. *Adv. Energy Mater.* **2020**, *10*, No. 2000493.
(56) Chai, D. D.; Yan, H. T.; Wang, X.; Li, X.; Fu, Y. Z. Retuning Solvating Ability of Ether Solvent by Anion Chemistry toward 4.5 V Class Li Metal Battery. *Adv. Funct. Mater.* **2024**, *34*, 10.
(57) Yu, Y.; Li, D.; Guo, Q.; Wang, M.; Zhang, H.; An, Q.; Cao, L. Anion-induced optimization of non-aqueous zinc-air battery performance: Insights into OTF-selection. *J. Power Sources* **2025**, *626*, No. 235764.
(58) González-Aguilera, L.; Vicent-Luna, J.; García-Balaguer, P.; Calero, S.; Madero-Castro, R.; Raymundo-Piñero, E.; Lu, X.; Gutiérrez, M.; Ferrer, M.; del Monte, F. Anion-rich solvation structures in high entropy aqueous electrolytes for supercapacitors with enlarged potential windows and superior rate capabilities. *J. Mater. Chem. A* **2025**, *13*, 31421−31434.
(59) Zhou, P.; Ou, Y.; Feng, Q.; Xia, Y.; Zhou, H.; Hou, W.; Song, X.; Lu, Y.; Yan, S.; Zhang, W.; He, Y.; Liu, K. Tuning the Nucleophilicity of Anion in Lithium Salt to Enable an Anion-Rich Solvation Sheath for Stable Lithium Metal Batteries. *Adv. Funct. Mater.* **2025**, *35*, 10.
(60) Erlich, R. H.; Popov, A. I. SPECTROSCOPIC STUDIES OF IONIC SOLVATION 0.10. STUDY OF SOLVATION OF SODIUM IONS IN NONAQUEOUS SOLVENTS BY NA-23 NUCLEAR MAGNETIC RESONANCE. *J. Am. Chem. Soc.* **1971**, *93*, 5620−5623.

(61) Kamlet, M. J.; Taft, R. W. SOLVATOCHROMIC COMPARISON METHOD 0.1. BETA-SCALE OF SOLVENT HYDROGEN-BOND ACCEPTOR (HBA) BASICITIES. *J. Am. Chem. Soc.* **1976**, *98*, 377−383.
(62) Reichardt, C.; Welton, T. *Solvents and Solvent Effects in Organic Chemistry*, 4th ed.; Wiley: Weinheim, Germany, 2011.
(63) Wu, Y. Z.; Hu, Q.; Liang, H. M.; Wang, A. P.; Xu, H.; Wang, L.; He, X. M. Electrostatic Potential as Solvent Descriptor to Enable Rational Electrolyte Design for Lithium Batteries. *Adv. Energy Mater.* **2023**, *13*, 6.
(64) Li, Z.; Li, W.; Li, Z.; Fu, J.; Chen, Q.; Yang, H.; Guo, X. Fluorine-oxygen co-coordination of lithium in fluorinated polymers for broad temperature quasi-solid-state batteries. *Nat. Commun.* **2025**, *16*, 9265.
(65) Chen, K.; Chen, H.; Zheng, Z.; Liu, Y.; Fang, Y.; Chen, Z.; Cao, Y. Identifying the Role of Solvation Entropy for the Solvation Chemistry in Nonaqueous Electrolytes. *Angew. Chem., Int. Ed.* **2025**, *64*, 9.
(66) Zhao, F.; Zhang, J.; Chen, J.; Gu, Z.; Fan, X.; Zhu, L.; Na, H.; Dong, M.; Guan, C.; Kong, L. Lithium Salt Association-Mediated Interfacial Charge Exchange for Low-Temperature Lithium-Metal Batteries: Beyond Lithium De-Solvation Manner. *Research* **2025**, *8*, 0802.
(67) Qi, H.; Liv, P. Solvation engineering in lithium-ion batteries: from fundamental mechanisms to electrolyte design. *Ionics* **2025**, *31*, 11409−11437.
(68) Peng, Z.; Ding, K.; Lai, M.; Qiu, R.; Xiao, Y.; Shi, J.; Guan, X.; Cai, Y.; Xu, C.; Wang, F.; Zheng, Q. Rational electrolyte solvent screening for high-energy lithium metal batteries at low temperatures. *Nat. Commun.* **2026**, *17*, 14.
(69) Niedermeyer, H.; Ashworth, C.; Brandt, A.; Welton, T.; Hunt, P. A. A step towards the a priori design of ionic liquids. *Phys. Chem. Chem. Phys.* **2013**, *15*, 11566−11578.
(70) Cerda-Monje, A.; Ormazabal-Toledo, R.; Cardenas, C.; Fuentealba, P.; Contreras, R. Regional Electrophilic and Nucleophilic Fukui Functions Efficiently Highlight the Lewis Acidic/Basic Regions in Ionic Liquids. *J. Phys. Chem. B* **2014**, *118*, 3696−3701.
(71) Wu, W. H.; Lu, Y. X.; Ding, H. R.; Peng, C. J.; Liu, H. L. The acidity/basicity of metal-containing ionic liquids: insights from surface analysis and the Fukui function. *Phys. Chem. Chem. Phys.* **2015**, *17*, 1339−1346.
(72) Liu, Y.; Wang, J. F. Lewis Acidity and Basicity of Mixed Chlorometallate Ionic Liquids: Investigations from Surface Analysis and Fukui Function. *Molecules* **2018**, *23*, 2516.
(73) Towers Tompkins, F. K.; Parker, L. G.; Fogarty, R. M.; Seymour, J. M.; Rowe, R.; Palgrave, R. G.; Matthews, R. P.; Bennett, R. A.; Hunt, P. A.; Lovelock, K. R. J. Efficient prediction of the local electronic structure of ionic liquids from low-cost calculations. *Phys. Chem. Chem. Phys.* **2025**, *27*, 8803−8812.
(74) Hu, H. P.; Shan, Y. Q.; Zhao, Q. M.; Wang, J. L.; Wu, L. J.; Liu, W. Q. The prediction of donor number and acceptor number of electrolyte solvent molecules based on machine learning. *J. Energy Chem.* **2024**, *98*, 374−382.
(75) Luo, H. R.; Gou, Q. Z.; Zheng, Y. J.; Wang, K. X.; Yuan, R. D.; Zhang, S. D.; Fang, W.; Luogu, Z.; Hu, Y. Z.; Mei, H. P.; Song, B. Y.; Sun, K.; Wang, J. H.; Li, M. Machine Learning-Assisted High-Donor-Number Electrolyte Additive Screening toward Construction of Dendrite-Free Aqueous Zinc-Ion Batteries. *ACS Nano* **2025**, *19*, 2427−2443.
(76) Zhan, Y. X.; Ren, X. J.; Zhao, S.; Guo, Z. L. Enhancing prediction of electron affinity and ionization energy in liquid organic electrolytes for lithium-ion batteries using machine learning. *J. Power Sources* **2025**, *629*, No. 235992.
(77) Gao, Y.; Qi, S.; Li, M.; Ma, T.; Song, H.; Cui, Z.; Liang, Z.; Du, L. Machine Learning Assisted Prediction of Donor Numbers: Guiding Rational Fabrication of Polymer Electrolytes for Lithium-Ion Batteries. *Angew. Chem., Int. Ed.* **2025**, *64*, No. e202411437.
(78) CAHEN, Y.; HANDY, P.; ROACH, E.; POPOV, A. SPECTROSCOPIC STUDIES OF IONIC SOLVATION. 16. LITHIUM-7 AND CHLORINE-35 NUCLEAR MAGNETIC-RESONANCE STUDIES IN VARIOUS SOLVENTS. *J. Phys. Chem.* **1975**, *79*, 80−85.
(79) Holoubek, J.; Yu, K.; Wu, J.; Wang, S.; Li, M.; Gao, H.; Hui, Z.; Hyun, G.; Yin, Y.; Mu, A.; Kim, K.; Liu, A.; Yu, S.; Pascal, T.; Liu, P.; Chen, Z. Toward a quantitative interfacial description of solvation for Li metal battery operation under extreme conditions. *Proc. Natl. Acad. Sci. U. S. A.* **2023**, *120*, No. e2310714120.
(80) Maciel, G. E.; Hancock, J. K.; Lafferty, L. F.; Mueller, P. A.; Musker, W. K. Lithium-7 Chemical Shifts of Lithium Perchlorate and Bromide in Various Solvents. *Inorg. Chem.* **1966**, *5*, 554−557.
(81) Briggs, D., Grant, J. T., Eds. *Surface Analysis by Auger and X-ray Photoelectron Spectroscopy*; IM Publications: Manchester, 2003.
(82) Lovelock, K. R. J.; Kolbeck, C.; Cremer, T.; Paape, N.; Schulz, P. S.; Wasserscheid, P.; Maier, F.; Steinrück, H. P. Influence of Different Substituents on the Surface Composition of Ionic Liquids Studied Using ARXPS. *J. Phys. Chem. B* **2009**, *113*, 2854−2864.
(83) Apperley, D. C.; Hardacre, C.; Licence, P.; Murphy, R. W.; Plechkova, N. V.; Seddon, K. R.; Srinivasan, G.; Swadźba-Kwaśny, M.; Villar-Garcia, I. J. Speciation of chloroindate(III) ionic liquids. *Dalton Trans.* **2010**, *39*, 8679−8687.
(84) Villar-Garcia, I. J.; Smith, E. F.; Taylor, A. W.; Qiu, F. L.; Lovelock, K. R. J.; Jones, R. G.; Licence, P. Charging of ionic liquid surfaces under X-ray irradiation: the measurement of absolute binding energies by XPS. *Phys. Chem. Chem. Phys.* **2011**, *13*, 2797−2808.
(85) Hurisso, B. B.; Lovelock, K. R. J.; Licence, P. Amino acid-based ionic liquids: using XPS to probe the electronic environment via binding energies. *Phys. Chem. Chem. Phys.* **2011**, *13*, 17737−17748.
(86) Taylor, A. W.; Men, S.; Clarke, C. J.; Licence, P. Acidity and basicity of halometallate-based ionic liquids from X-ray photoelectron spectroscopy. *RSC Adv.* **2013**, *3*, 9436−9445.
(87) Currie, M.; Estager, J.; Licence, P.; Men, S.; Nockemann, P.; Seddon, K. R.; Swadźba-Kwaśny, M.; Terrade, C. Chlorostannate(II) Ionic Liquids: Speciation, Lewis Acidity, and Oxidative Stability. *Inorg. Chem.* **2013**, *52*, 1710−1721.
(88) Villar-Garcia, I. J.; Lovelock, K. R. J.; Men, S.; Licence, P. Tuning the electronic environment of cations and anions using ionic liquid mixtures. *Chem. Sci.* **2014**, *5*, 2573−2579.
(89) Men, S. A.; Lovelock, K. R. J.; Licence, P. X-ray photoelectron spectroscopy of trihalide ionic liquids: Comparison to halide-based analogues, anion basicity and beam damage. *Chem. Phys. Lett.* **2017**, *679*, 207−211.
(90) Fogarty, R. M.; Matthews, R. P.; Ashworth, C. R.; Brandt-Talbot, A.; Palgrave, R. G.; Bourne, R. A.; Vander Hoogerstraete, T.; Hunt, P. A.; Lovelock, K. R. J. Experimental validation of calculated atomic charges in ionic liquids. *J. Chem. Phys.* **2018**, *148*, No. 193817.
(91) Fogarty, R. M.; Rowe, R.; Matthews, R. P.; Clough, M. T.; Ashworth, C. R.; Brandt, A.; Corbett, P. J.; Palgrave, R. G.; Smith, E. F.; Bourne, R. A.; Chamberlain, T. W.; Thompson, P. B. J.; Hunt, P. A.; Lovelock, K. R. J. Atomic charges of sulfur in ionic liquids: experiments and calculations. *Faraday Discuss.* **2018**, *206*, 183−201.
(92) Seymour, J. M.; Gousseva, E.; Towers Tompkins, F. K.; Parker, L. G.; Alblewi, N. O.; Clarke, C. J.; Hayama, S.; Palgrave, R. G.; Bennett, R. A.; Matthews, R. P.; Lovelock, K. R. J. Unravelling the complex speciation of halozincate ionic liquids using X-ray spectroscopies and calculations. *Faraday Discuss.* **2024**, *253*, 251−272.
(93) Longo, L. S.; Smith, E. F.; Licence, P. Study of the Stability of 1-Alkyl-3-methylimidazolium Hexafluoroantimonate(V) Based Ionic Liquids Using X-ray Photoelectron Spectroscopy. *ACS Sustain. Chem. Eng.* **2016**, *4*, 5953−5962.
(94) May, B.; Honle, M.; Heller, B.; Greco, F.; Bhuin, R.; Steinrück, H. P.; Maier, F. Surface-Induced Changes in the Thermochromic Transformation of an Ionic Liquid Cobalt Thiocyanate Complex. *J. Phys. Chem. Lett.* **2017**, *8*, 1137−1141.
(95) Seymour, J. M.; Gousseva, E.; Parker, L. G.; Towers Tompkins, F. K.; Fogarty, R. M.; Frankemoelle, L.; Rowe, R.; Clarke, C. J.; Duncan, D. A.; Palgrave, R. G.; Bennett, R. A.; Hunt, P. A.; Lovelock, K. R. J. d10s2 Post-Transition Metal Anions: Identifying and

Analyzing Their Dual-Mode Lewis Basicity. *J. Phys. Chem. Lett.* **2025**, *16*, 2831−2836.
(96) Winter, B.; Faubel, M. Photoemission from liquid aqueous solutions. *Chem. Rev.* **2006**, *106*, 1176−1211.
(97) Ottosson, N.; Vacha, R.; Aziz, E. F.; Pokapanich, W.; Eberhardt, W.; Svensson, S.; Öhrwall, G.; Jungwirth, P.; Björneholm, O.; Winter, B. Large variations in the propensity of aqueous oxychlorine anions for the solution/vapor interface. *J. Chem. Phys.* **2009**, *131*, No. 124706.
(98) Seidel, R.; Winter, B.; Bradforth, S. E. Valence Electronic Structure of Aqueous Solutions: Insights from Photoelectron Spectroscopy. *Annu. Rev. Phys. Chem.* **2016**, *67*, 283−305.
(99) Gaiduk, A. P.; Govoni, M.; Seidel, R.; Skone, J. H.; Winter, B.; Galli, G. Photoelectron Spectra of Aqueous Solutions from First Principles. *J. Am. Chem. Soc.* **2016**, *138*, 6912−6915.
(100) Pham, T. A.; Govoni, M.; Seidel, R.; Bradforth, S. E.; Schwegler, E.; Galli, G. Electronic structure of aqueous solutions: Bridging the gap between theory and experiments. *Sci. Adv.* **2017**, *3*, 8.
(101) Towers Tompkins, F. K.; Gousseva, E.; Bennett, R. A.; Grau-Crespo, R.; Lovelock, K. R. J. Core-level binding energies describe electrostatic potentials at nuclei for ionic liquids. *Phys. Chem. Chem. Phys.* **2025**, *27*, 22004−22012.
(102) Marcus, Y. THE PROPERTIES OF ORGANIC LIQUIDS THAT ARE RELEVANT TO THEIR USE AS SOLVATING SOLVENTS. *Chem. Soc. Rev.* **1993**, *22*, 409−416.
(103) Pike, S. J.; Lavagnini, E.; Varley, L. M.; Cook, J. L.; Hunter, C. A. H-Bond donor parameters for cations. *Chem. Sci.* **2019**, *10*, 5943−5951.
(104) McGrogan, A.; Lafferty, J.; O'Neill, L.; Brown, L.; Young, J. M.; Goodrich, P.; Muldoon, M. J.; Moura, L.; Youngs, S.; Hughes, T. L.; Gärtner, S.; Youngs, T. G. A.; Holbrey, J. D.; Swadzba-Kwasny, M. Liquid Structure of Ionic Liquids with NTf_2 ⁻ Anions, Derived from Neutron Scattering. *J. Phys. Chem. B* **2024**, *128*, 3220−3235.
(105) Gumaste, T.; Cooper, F.; Blakemore, J. Analysis of Bis(trifluoromethylsulfonyl)imide Interactions with Metal Cations Through a Chemical Informatics Approach. *Molecules* **2026**, *31*, 18.
(106) Best, S. A.; Walton, R. A. X-RAY PHOTOELECTRON-SPECTRA OF INORGANIC MOLECULES. 19. THIOCYANATO AND ISOTHIOCYANATO COMPLEXES OF TRANSITION-METALS - CARBON-1S, NITROGEN-1S AND SULFUR-2P BINDING-ENERGIES AND THEIR POSSIBLE CORRELATION WITH MODE OF THIOCYANATE BONDING. *Isr. J. Chem.* **1976**, *15*, 160−164.
(107) Lovelock, K. R. J.; Villar-Garcia, I. J.; Maier, F.; Steinrück, H. P.; Licence, P. Photoelectron Spectroscopy of Ionic Liquid-Based Interfaces. *Chem. Rev.* **2010**, *110*, 5158−5190.
(108) Lovelock, K. R. J.; Licence, P. In *Ionic Liquids UnCOILed: Critical Expert Overviews*; Seddon, K. R., Plechkova, N. V., Eds.; Wiley: Oxford, 2012; Chapter 8, pp 251−282.
(109) Steinrück, H. P. Recent developments in the study of ionic liquid interfaces using X-ray photoelectron spectroscopy and potential future directions. *Phys. Chem. Chem. Phys.* **2012**, *14*, 5010−5029.
(110) Erdmann, P.; Greb, L. What Distinguishes the Strength and the Effect of a Lewis Acid: Analysis of the Gutmann-Beckett Method. *Angew. Chem., Int. Ed.* **2022**, *61*, No. e202114550.
(111) Stoess, L.; Greb, L. What distinguishes the strength and the effect of a Lewis base: insights with a strong chromogenic silicon Lewis acid. *Chem. Sci.* **2025**, *16*, 15387−15395.
(112) Cláudio, A. F. M.; Swift, L.; Hallett, J. P.; Welton, T.; Coutinho, J. A. P.; Freire, M. G. Extended scale for the hydrogen-bond basicity of ionic liquids. *Phys. Chem. Chem. Phys.* **2014**, *16*, 6593−6601.
(113) Gousseva, E.; Midgley, S. D.; Seymour, J. M.; Seidel, R.; Grau-Crespo, R.; Lovelock, K. R. J. Understanding X-ray Photoelectron Spectra of Ionic Liquids: Experiments and Simulations of 1-Butyl-3-methylimidazolium Thiocyanate. *J. Phys. Chem. B* **2022**, *126*, 10500−10509.
(114) Towers Tompkins, F. K.; Parker, L. G.; Fogarty, R. M.; Seymour, J. M.; Gousseva, E.; Grinter, D. C.; Palgrave, R. G.; Smith, C. D.; Bennett, R. A.; Matthews, R. P.; Lovelock, K. R. J. Controlling and predicting alkyl-onium electronic structure. *Chem. Commun.* **2024**, *60*, 10756−10759.
(115) Philippi, F.; Middendorf, M.; Shigenobu, K.; Matsuyama, Y.; Palumbo, O.; Pugh, D.; Sudoh, T.; Dokko, K.; Watanabe, M.; Schoenhoff, M.; Shinoda, W.; Ueno, K. Evolving better solvate electrolytes for lithium secondary batteries. *Chem. Sci.* **2024**, *15*, 7342−7358.
(116) Pokorny, D.; Syrovy, T.; Klikar, M.; Parík, P.; Buresová, Z.; Rehácková, L.; Bures, F. Tailoring lithium dicyanoimidazolide: structure-property relationships. *Mater. Adv.* **2026**, *7*, 3875−3884.
(117) Niedzicki, L.; Karpierz, E.; Zawadzki, M.; Dranka, M.; Kasprzyk, M.; Zalewska, A.; Marcinek, M.; Zachara, J.; Domanska, U.; Wieczorek, W. Lithium cation conducting TDI anion-based ionic liquids. *Phys. Chem. Chem. Phys.* **2014**, *16*, 11417−11425.
(118) Zavalij, P.; Yang, S.; Whittingham, M. Structures of potassium, sodium and lithium bis(oxalato)borate salts from powder diffraction data. *Acta Crystallogr. Sect. B-Struct. Commun.* **2003**, *59*, 753−759.
(119) Galabov, B.; Ilieva, S.; Koleva, G.; Allen, W. D.; Schaefer, H. F.; von R. Schleyer, P. Structure-reactivity relationships for aromatic molecules: electrostatic potentials at nuclei and electrophile affinity indices. *Wiley Interdiscip. Rev.-Comput. Mol. Sci.* **2013**, *3*, 37−55.
(120) Suresh, C. H.; Remya, G. S.; Anjalikrishna, P. K. Molecular electrostatic potential analysis: A powerful tool to interpret and predict chemical reactivity. *Wiley Interdiscip. Rev.-Comput. Mol. Sci.* **2022**, *12*, No. e1601.
(121) Suresh, C. H.; Anila, S. Molecular Electrostatic Potential Topology Analysis of Noncovalent Interactions. *Acc. Chem. Res.* **2023**, *56*, 1884−1895.
(122) Asl, H.; Manthiram, A. Reining in dissolved transition-metal ions. *Science* **2020**, *369*, 140−141.
(123) Fogarty, R. M.; Matthews, R. P.; Hunt, P. A.; Lovelock, K. R. J. Accurate prediction of ionic liquid density-of-states from low-cost calculations. *Phys. Chem. Chem. Phys.* **2025**, *27*, 9068−9075.
(124) Fogarty, R. M.; Palgrave, R. G.; Bourne, R. A.; Handrup, K.; Villar-Garcia, I. J.; Payne, D. J.; Hunt, P. A.; Lovelock, K. R. J. Electron spectroscopy of ionic liquids: experimental identification of atomic orbital contributions to valence electronic structure. *Phys. Chem. Chem. Phys.* **2019**, *21*, 18893−18910.
(125) Seymour, J. M.; Gousseva, E.; Large, A. I.; Clarke, C. J.; Licence, P.; Fogarty, R. M.; Duncan, D. A.; Ferrer, P.; Venturini, F.; Bennett, R. A.; Palgrave, R. G.; Lovelock, K. R. J. Experimental measurement and prediction of ionic liquid ionisation energies. *Phys. Chem. Chem. Phys.* **2021**, *23*, 20957−20973.
(126) Grinter, D.; Ferrer, P.; Venturini, F.; van Spronsen, M.; Large, A.; Kumar, S.; Jaugstetter, M.; Iordachescu, A.; Watts, A.; Schroeder, S.; Kroner, A.; Grillo, F.; Francis, S.; Webb, P.; Hand, M.; Walters, A.; Hillman, M.; Held, G. VerSoX B07-B: a high-throughput XPS and ambient pressure NEXAFS beamline at Diamond Light Source. *J. Synchrot. Radiat.* **2024**, *31*, 578−589.
(127) Seidel, R.; Pohl, M. N.; Ali, H.; Winter, B.; Aziz, E. F. Advances in liquid phase soft-x-ray photoemission spectroscopy: A new experimental setup at BESSY II. *Rev. Sci. Instrum.* **2017**, *88*, No. 073107.
(128) Zhu, S.; Scardamaglia, M.; Kundsen, J.; Sankari, R.; Tarawneh, H.; Temperton, R.; Pickworth, L.; Cavalca, F.; Wang, C.; Tissot, H.; Weissenrieder, J.; Hagman, B.; Gustafson, J.; Kaya, S.; Lindgren, F.; Källquist, I.; Maibach, J.; Hahlin, M.; Boix, V.; Gallo, T.; Rehman, F.; D'Acunto, G.; Schnadt, J.; Shavorskiy, A. HIPPIE: a new platform for ambient-pressure X-ray photoelectron spectroscopy at the MAX IV Laboratory. *J. Synchrot. Radiat.* **2021**, *28*, 624−636.
(129) Rueff, J.; Ablett, J.; Céolin, D.; Prieur, D.; Moreno, T.; Balédent, V.; Lassalle-Kaiser, B.; Rault, J.; Simon, M.; Shukla, A. The GALAXIES beamline at the SOLEIL synchrotron: inelastic X-ray scattering and photoelectron spectroscopy in the hard X-ray range. *J. Synchrot. Radiat.* **2015**, *22*, 175−179.

(130) Frisch, M. J.; Trucks, G. W.; Schlegel, H. B.; Scuseria, G. E.; Robb, M. A.; Cheeseman, J. R.; Scalmani, G.; Barone, V.; Petersson, G. A.; Nakatsuji, H.; Li, X.; Caricato, M.; Marenich, A. V.; Bloino, J.; Janesko, B. G.; Gomperts, R.; Mennucci, B.; Hratchian, H. P.; Ortiz, J. V.; Izmaylov, A. F.; Sonnenberg, J. L.; Williams-Young, D.; Ding, F.; Lipparini, F.; Egidi, F.; Goings, J.; Peng, B.; Petrone, A.; Henderson, T.; Ranasinghe, D.; Zakrzewski, V. G.; Gao, J.; Rega, N.; Zheng, G.; Liang, W.; Hada, M.; Ehara, M.; Toyota, K.; Fukuda, R.; Hasegawa, J.; Ishida, M.; Nakajima, T.; Honda, Y.; Kitao, O.; Nakai, H.; Vreven, T.; Throssell, K.; Montgomery, J. J. A.; Peralta, J. E.; Ogliaro, F.; Bearpark, M. J.; Heyd, J. J.; Brothers, E. N.; Kudin, K. N.; Staroverov, V. N.; Keith, T. A.; Kobayashi, R.; Normand, J.; Raghavachari, K.; Rendell, A. P.; Burant, J. C.; Iyengar, S. S.; Tomasi, J.; Cossi, M.; Millam, J. M.; Klene, M.; Adamo, C.; Cammi, R.; Ochterski, J. W.; Martin, R. L.; Morokuma, K.; Farkas, O.; Foresman, J. B.; Fox, D. J. *Gaussian 16*, revision C.01; Gaussian, Inc., 2016.

(131) Fairley, N.; Fernandez, V.; Richard-Plouet, M.; Guillot-Deudon, C.; Walton, J.; Smith, E.; Flahaut, D.; Greiner, M.; Biesinger, M.; Tougaard, S.; Morgan, D.; Baltrusaitis, J. Systematic and collaborative approach to problem solving using X-ray photoelectron spectroscopy. *Appl. Surf. Sci. Adv.* **2021**, *5*, No. 100112.

(132) Kolbeck, C.; Killian, M.; Maier, F.; Paape, N.; Wasserscheid, P.; Steinrück, H. P. Surface characterization of functionalized imidazolium-based ionic liquids. *Langmuir* **2008**, *24*, 9500−9507.

https://doi.org/10.1021/jacs.6c06567
J. Am. Chem. Soc. 2026, 148, 35498−35514